POLITECNICO DI TORINO

Master's Degree in Communications Engineering

Master's Degree Thesis

Enhancing Digital Twin Transmission Model to Enable Optical Network Infrastructure as a Service

Academic Supervisors

Prof. Vittorio CURRI

Ing. Renato AMBROSONE

Candidate

Enrico MIOTTO

Company Supervisor
Consortium GARR

Ing. Paolo BOLLETTA

October 2024

Abstract

In the dynamic landscape of telecommunications, optical networks have become the backbone of high-speed data transmission systems, reshaping global information flow. In response to the proliferation of data-intensive applications, there's an unprecedented demand for bandwidth. Optical networks effectively address this need with their high data-carrying capacity.

To optimize and share this pervasive infrastructure, there's a call for the progressive introduction of disaggregation and openness in optical networking. This involves separating the control plane from the data plane, as per the software defined networking (SDN) paradigm, enabling virtualized infrastructure slicing and sharing. To reach this scope, open control protocols and models are crucial, as is the optical network controller's ability to dynamically optimize the data and control plane. Optical networking, grounded in Wavelength Division Multiplexing (WDM) optical circuits on a transparent optical infrastructure, requires full virtualization of the physical layer for optimal, dynamic, and software-defined exploitation of optical networks. Openness enables the possibility to implement an optical network digital twin (DT). In general, the DT of a system can be defined as a set of methods relying on data sensed from the system that allows an accurate simulation of the actual system functionalities. So, the DT is the core for an optimized software-defined management of a complex system. The virtualization and SDN, achieved thanks to the DT development, allow the exploitation of Network-as-a-Service paradigm (NaaS). NaaS enables a more agile and cost-effective network deployment, allowing organizations to scale their infrastructure based on demand. This flexibility is crucial, as it empowers businesses to adapt to changing requirements and market dynamics. Moreover, the implementation of multivendor infrastructure addresses interoperability challenges, fostering a competitive market environment. This not only promotes innovation but also mitigates vendor lock-in, enabling organizations to select and integrate the leading-edge solutions.

In the framework of open and disaggregated optical networks architectures, re-configurable add/drop multiplexers (ROADMs), based on wavelength selective switches (WSSs) technologies, providing switching at optical level, are key elements to be inspected and analysed, in the development of an optical network DT. Liquid-Crystal on Silicon (LCoS) spatial light modulator (SLM) technologies, which constitute the base component of WSSs, introduce most of the Polarization Dependent Loss (PDL) in optical systems that results in a relative degradation of signal-to-noise ratio (SNR). Depending both on frequency and ports, the PDL introduced by each WSS must be treated as a random variable in the vast majority of use cases, where a full characterization of all the WSSs is not available and not feasible. In this scenario, a worst-case value of PDL can be considered for evaluating a conservative SNR penalty. This value is commonly provided in WSS datasheets,

therefore the usual paradigm is to treat PDL as if it introduced the maximum impairment. The limitation of this approach is that often the conservative estimate of PDL is not efficient, since PDL penalty strongly depends on the optical system and, in general, it is way lower than the conservative estimate. As a consequence, while guaranteeing the correct system operation, the conservative approach results in a waste of resources. Based on the previous assertions, there is the need of a more accurate model for the estimation of PDL-induced penalty, with an accurate and efficient estimation of the system margins.

The work of this thesis focuses on PDL mathematical modelling, deriving statistical tools to determine a penalty in term of SNR. The clear guideline of all the work has been the objective to provide a new tool to deal with disaggregation, in the context of the enhancement of "GNPy" DT transmission model developed in PLANET team of OptCom research group of Politecnico di Torino. In treating the PDL problem, special attention has been dedicated to how PDL acts on noise introduced along the path, since each noise contribution experiences a different effect in term of PDL, crossing a different number of WSS. In addition, also Digital Signal Processing (DSP) effect has been taken into account, considering that the distortion applied on the dual polarization (DP) information signal by the PDL is totally recovered by DSP, while noise's distortion is not, since noise is, in general, introduced along the path and it does not experience the entire link PDL. The key idea behind all the developed framework is to exploit the description of PDL effect on noise given by power transfer matrices, underlining the evolution of the noise polarization state from the power point of view. The proposed model has been validated through an experimental analysis carried out at LINKS Foundation laboratories, in order to assess the goodness and the effectiveness of the adopted paradigm. The laboratory analysis has been carried out in three steps in order to characterize first the PDL of each device and then of the entire system. Finally, a transceiver has been inserted and some noise sources distributed along the considered path. In conclusion, an extensive Monte Carlo investigation has been performed, in order to validate the mathematical model and to inspect the case in which a large number of PDL elements are posed in cascade along a lightpath, both when PDL is uniformly introduced by the devices, and also when its value comes from a distribution of probability, which is the case closer to the reality.

"It is love, not reason, that is stronger than death"
Thomas Mann, Der Zauberberg

Acknowledgements

This thesis work would not have existed without the help and the support of many people. Therefore, it is a due step to thank all those who made it possible.

First I have to thank all the PLANET team whom I have had the pleasure of collaborating with along this journey. In particular, I want to thank my supervisors prof. Vittorio Curri for his trust in me and for the opportunities he provided me, and Renato Ambrosone for his endless helpfulness and friendship that he has always shown me.

The pillar of this thesis is undoubtedly the past work on Polarization Dependent Loss, which Andrea D'Amico carried out during his PhD at PLANET team. Thank you for the patience and the continuous help that you provided me, solving my doubts even if you were on the other side of the ocean. I was able to continue your past work because I stood on the shoulders of a giant.

Regarding the laboratory activity, my thanks go to Stefano Straullu and Francesco Aquilino of LINKS Foundation laboratories, who have expertly supported me with enormous kindness and competence. It has been deeply formative for me working with you.

This work has been developed as part of the "Accordo Attuativo": Building and Automate Long Lasting Open Optical Networking (BALLOON) between Consortium GARR and Politecnico di Torino. Great thanks to the BALLOON team people Paolo Bolletta, Gloria Vuagnin and Matteo Colantonio.

Finally, I would like to dedicate this thesis to my dear family: your love guided me through all the difficulties I faced.

I dedicate my effort also to the memory of my grandparents, whom I miss painfully.

If you watch over me from somewhere, I hope I have made you proud of me.

Table of Contents

List of Tables

List of Figures

Acronyms

API Application Programming Interfaces

ASE Amplified Spontaneous Emission

AWGN Additive White Gaussian Noise

BER Bit Error Rate

DEMUX Demultiplexer

DP-QPSK Dual Polarization Quadrature Phase Shift Keying

DSP Digital Signal Processing

DT digital twin

EDFA Erbium Doped Fiber Amplifier

GNPy Gaussian Noise in Phyton

GPIB General Purpose Interface Bus

GSNR Generalized Signal to Noise Ratio

IoT Internet of Things

ISNR Inverse Signal to Noise Ratio

LCoS Liquid Crystal on Silicon

MUX Multiplexer

NaaS Network as a Service

NLI Non Linear Interference

OLS Optical Line System

ONC Optical Network Controller

OON Open Optical Network

OSNR Optical Signal to Noise Ratio

PDF Probability Density Function

PDL Polarization Dependent Loss

QoT Quality of Transmission

QPSK Quadrature Phase Shift Keying

ROADM Reconfigurable Optical Add Drop Multiplexer

RX Receiver

SDN Software Defined Networking

SNR Signal to Noise Ratio

TIP Telecom Infra Project

TX Transceiver

VOA Variable Optical Attenuator

WDM Wavelength Division Multiplexing

WSS Wavelength Selective Switch

WXC Wavelength Cross-Connect

XT Crosstalk

Chapter 1

Introduction

Optical Networks are critical infrastructures which play a significant role in modern communications. Their massive capacity and high bandwidth availability are pivotal in ensuring digital services in an increasingly connected world. Optical Networks are complex systems, based on optical fibers. Their resistance to electromagnetic interference and signal degradation, coupled with scalability, meets the evolving needs of communication infrastructure. As internet traffic continues to surge due to the rapid growth of connected devices, the rising demand for data-intensive applications like video streaming, cloud computing, and Internet of Things (IoT), along with the deployment of 5G networks [1], optical networks are expected to handle this increasing data traffic demand. Energy efficiency is another advantage, with optical communication consuming less power compared to traditional electronic methods, contributing to environmental friendliness [2].

An optical network is a meshed, ring or tree topology of switching nodes connected by a set of Optical Line Systems (OLSs). An OLS, as depicted in Figure 2.1, is a point-to-point optical transparent bidirectional link connecting two switching nodes [3]. Transparency, in optical networking, means that the considered link is all-optical from end to end without any electrical switching in the middle [4]. Its main component are bidirectional fiber pairs, in-line amplifiers and booster amplifiers. A node in an Optical Network is a site including devices able to address the incoming optical signals to a selected output. The node degree is the number of OLS connected to the node itself.

Optical switching in a network node is based on transparent wavelength routing i.e. each incoming signal in the WDM spectrum can be selectively addressed to any output. Wavelength can be added and dropped within the node, relying on a device called Reconfigurable Optical Add Drop Multiplexer (ROADM) [5]. These devices allow for dynamic and remote-controlled deployment of lightpaths, so that operators can remotely control the routing and switching of wavelengths, enabling on-demand reconfiguration of optical connections. In a ROADM, any

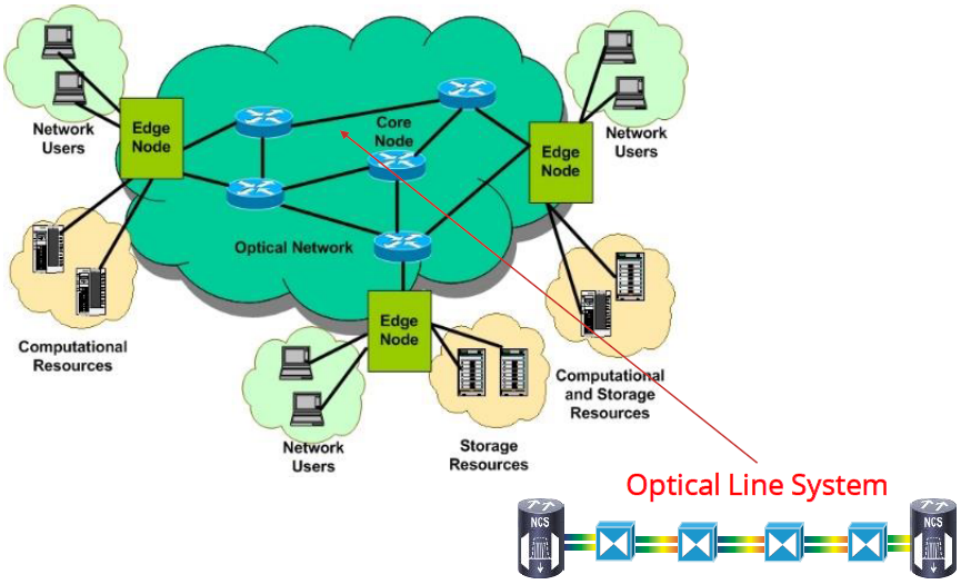

Figure 1.1: Optical Line System in an Optical Network

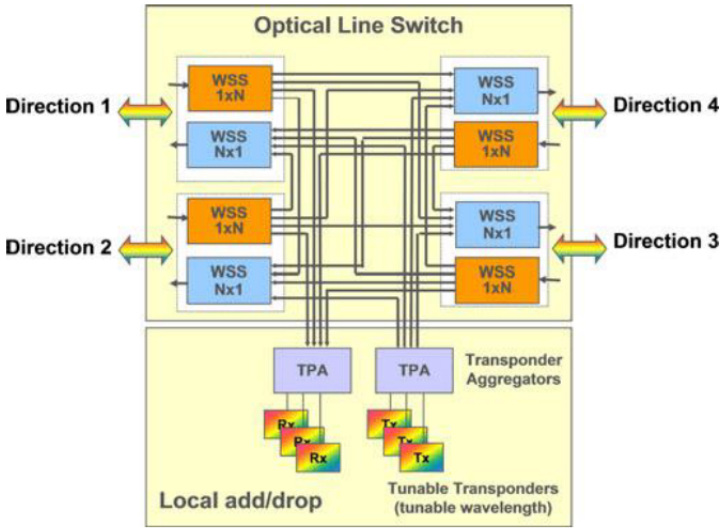

Figure 1.2: Reconfigurable Optical Add Drop Multiplexer

input wavelength can be switched to any output port in a transparent way [6].

The signal crossing the Optical Network can be seen as a transparent path at a given wavelength. For the involved transceivers a lightpath is a dedicated channel

from source to destination. It needs the availability of the same wavelength on all the crossed OLS (wavelength continuity) and the capability to be proper switched by all the crossed switches.

1.1 Software Defined Optical Networking

To improve the infrastructure exploitation, the pursued solution is the application of Software Defined Networking (SDN) approach at the physical layer [7]. Traditionally, SDN approach builds each network element upon three architectural planes [8], which are depicted in Figure 1.3:

- **Control plane**: in charge of computing the local forwarding state.
- **Data plane**: processing and delivery of packets with local forwarding state.
- **Management plane**: in purpose of providing interfaces towards a human figure who must interact with the device.

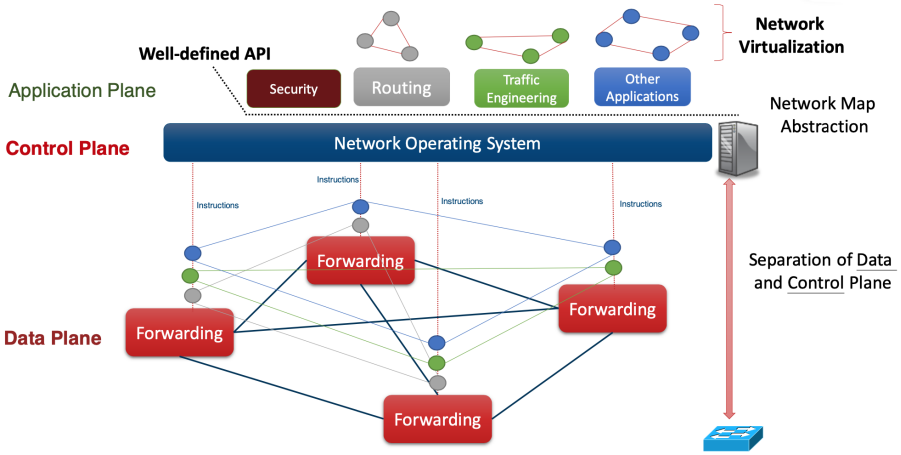

Figure 1.3: SDN paradigm

To perform routing and wavelength assignment in Optical Networks, according to the SDN paradigm, a centralized Optical Network Controller (ONC) needs full topology knowledge, full control on the network status and full abstraction on physical Quality of Transmission (QoT) to activate the maximum transmission capacity on the established optical circuit (lightpath). The advantages provided by a ONC are well known in literature [9]. The ONC relies on an abstraction of the transparent Optical Network, allowing the operators to remotely monitor and adjust the routing of wavelengths, eliminating the need for manual interventions at physical network nodes.

Modern transport network relies on IP on WDM approach. IP virtual network topology may be different from the physical one, and it is defined by routing tables according to the packet switching paradigm [10]. The IP virtual network lies on the optical transport network, which is composed by reconfigurable optical switches, ensuring the circuit-switching approach to the WDM transport.

In this scenario, to optimize and share this pervasive infrastructure, there's a call for the progressive introduction of disaggregation and openness in optical networking [11]. This, according to the mentioned SDN paradigm, involves separating the control plane from the data plane, enabling virtualized infrastructure slicing and sharing. In order to reach this scope, open control protocols and models are crucial, as is the ONC's ability to dynamically optimize the data and control plane. Actually there are not standard solutions to control the hardware, but a standard solution to do that on transport operation does exist, which is provided by Open Flow [12].

1.2 Open Optical Networking

Openness on Optical Networks refers to the interoperability, standardization and collaboration among vendors. This is achieved through the adoption of general-purpose hardware and shared (open) protocols, exploiting the disaggregation applied to the Optical Network hierarchical structure. Three approaches are possible in term of network disaggregation [13]:

- **Fully Aggregated Optical Network**: Solution that does not exploit SDN below layer 2 and where all the entire trasnport network is seen as a single managed system.
- **Fully Disaggregated Optical Network**: each device is a separate network element, which is independently controlled.
- **Partially Disaggregated Optical Network**: network elements are transponders and OLSs, that are controlled through dedicated Application Programming Interfaces (API).

Currently the most adopted solution is the partially disaggregated one, which is a trade-off between the advantageous but complex fully disaggregated approach and the inefficient but simpler fully aggregated one.

As already mentioned, openness is related to how the network elements, in a partially disaggregated approach, are able to cooperate through open control protocols and API. If closed solutions are adopted, hardware must be of the same vendor in order to deploy the transport network. On the other hand, openness

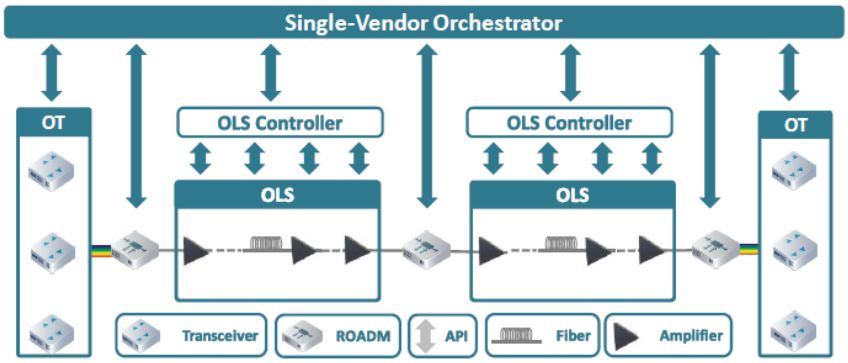

Figure 1.4: single-vendor partially disaggregated scenario

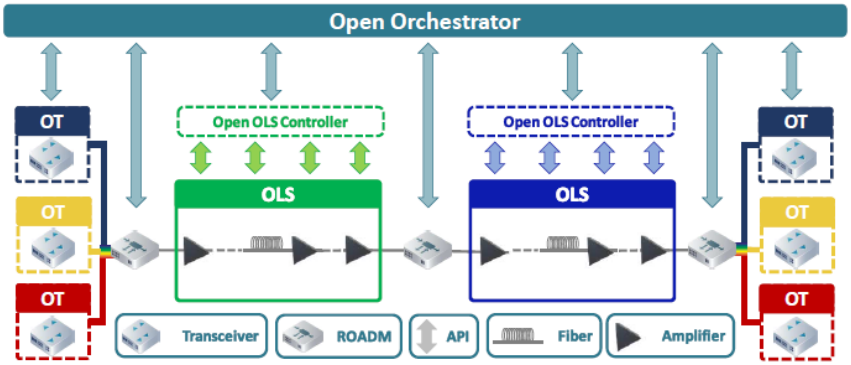

Figure 1.5: multi-vendor partially disaggregated scenario

allows multi-vendor devices to interoperate. The difference between open and closed approach is depicted in Figure 1.4 and Figure 1.5.

In order to perform network elements control and management an accurate theoretical abstraction must be adopted. In addition, each network element must be reachable and controlled bi open protocols and API.

The network can be abstracted as a weighted graph with respect to the transparent signal propagation on each crossed network element. Over the lightpath the wavelength accumulates impairments [14]. Through this abstraction, openness enables the possibility to implement an Optical Network digital twin (DT).

1.3 Optical Network Digital Twin

The first definition of the digital twin (DT) was proposed by NASA as an ”integrated multi-physics, multi-scale, probabilistic simulation system that uses the best

available physical models and sensor updates" [15]. Then, the concept has been extensively used in several fields adapting the definition to each specific application. In general, the DT of a system can be defined as a set of methods relying on data sensed from the system that allows an accurate simulation of the actual system functionalities. So, the DT is the core for an optimized software-defined management of a complex system [16].

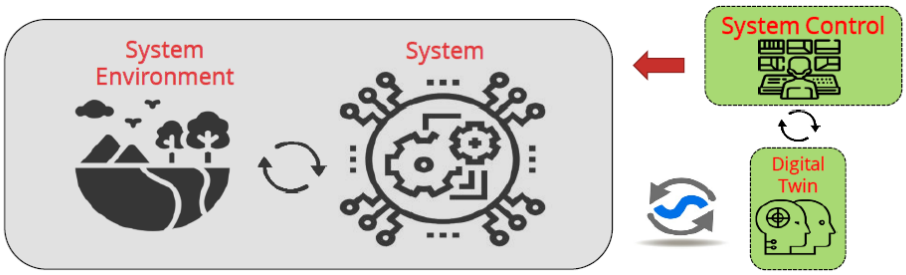

Figure 1.6: Digital Twin

In Figure 1.6 the environment in which a DT operates is depicted. The system and the system environment (also called "real twin") are emulated by the DT, which tells the ONC what to expect based on the information collected by sensors and interfaces in real time. Based on the DT simulation, the controller is able to act on the system effectively, making it working in the desired way.

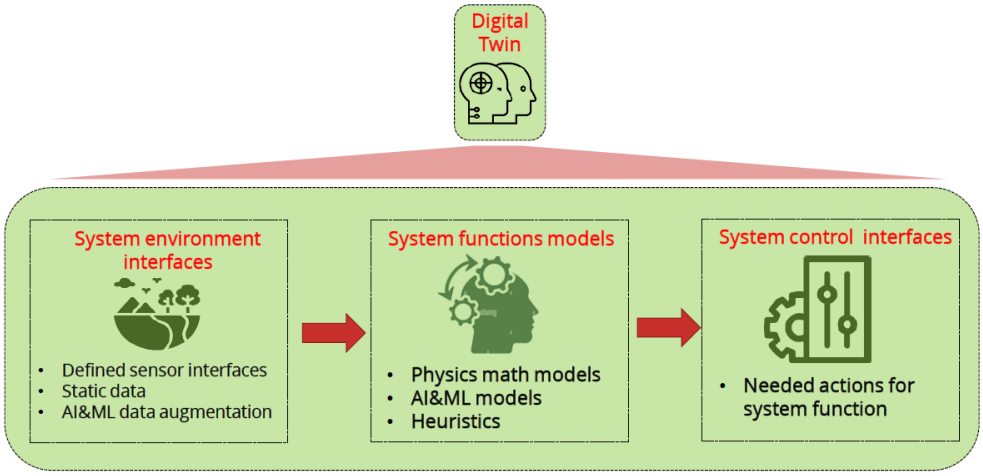

Figure 1.7: Inside a Digital Twin

Many building blocks are needed to develop a DT: the most important ones are shown in Figure 1.7. In this thesis work the focus will be on the system function

models, without delving into environment and control interfaces. The DT relies on very accurate and complex mathematical and physical models, through which it is able to predict the system behaviour, based on what is collected by sensors. The more precise and complete are the models, the higher is the fidelity when the system is simulated. Therefore, the enhancement of the DT models is pivotal in determining a good result in term of its performance. This is achieved through the theoretical derivation and experimental validation of new mathematical models, enabling new features and improving the DT efficiency and completeness.

Applying the concept of DT to Optical Networks it is possible to develop a tool suited both for the design and the control of networks functionalities. Namely, this approach is based on the concept of *physical layer aware networking*, exploiting the DT to take into consideration physical layer impairments and let the ONC act to manage the network effectively. To build the physical layer abstraction mentioned before, transparent lightpath are well approximated as dual polarization AWGN coherent channels [14]. The situation depicted in Figure 1.8, where a lightpath is abstracted as a point-to-point system composed by TX, RX and experiencing impairments due to the physical effects introduced along the path [17].

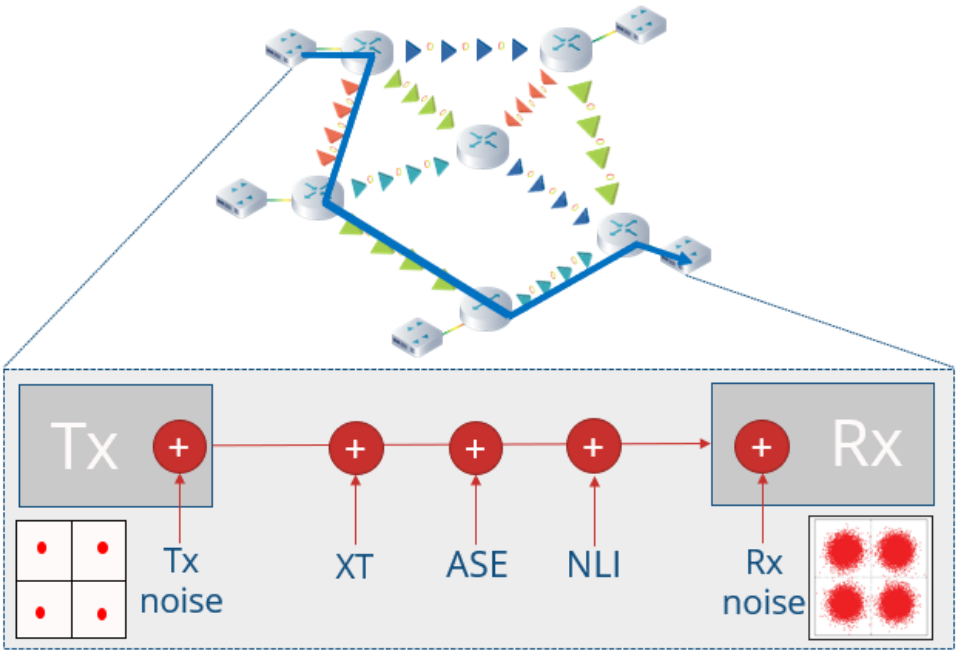

Figure 1.8: Physical layer abstraction

A unique parameter identifies the QoT along the path, which is typically defined as the Generalized Signal to Noise Ratio (GSNR) [18].

$$GSNR = \frac{P_\lambda}{P_{ASE;\lambda} + P_{NLI;\lambda} + P_{XT;\lambda}} \tag{1.1}$$

In the example provided in Equation 1.1 the considered impairments for GSNR are respectively Amplified Spontaneous Emission, Non Linear Interference and Crosstalk. In the prosecution another type of physical effect, named Polarization Dependent Loss (PDL) will become the object of the discussion through an extensive mathematical modeling and model validation.

The concept of GSNR is useful since each optical network element can be abstracted as introducing some amount of Gaussian disturbance on the signal. So, each lightpath is well modelled as an AWGN channel. GSNR definition has benn then introduced specifically to describe the SNR metric for transparent lightpaths in an optical network. Such situation is exemplified in Figure 1.9.

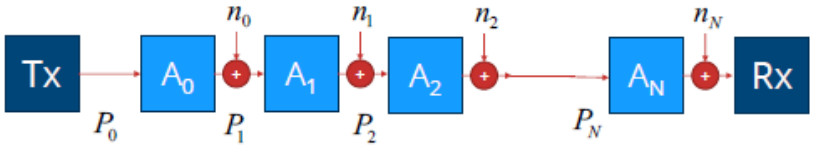

Figure 1.9: Cascade of noisy components to represent propagation over a transparent lightpath

To compute the GSNR in the case of Figure 1.9, it is necessary to propagate each noise contribution to the end of the link, taking into account the corresponding attenuation that it experiences along the path:

$$GSNR = \frac{P_0 \cdot A_0 ... A_N}{P_{n0} \cdot A_1 ... A_N + P_{n1} \cdot A_2 ... A_N + ... + P_{nN}} \tag{1.2}$$

$$ISNR = \frac{1}{GSNR} = \frac{P_{n0} \cdot A_1 ... A_N + P_{n1} \cdot A_2 ... A_N + ... + P_{nN}}{P_0 \cdot A_0 ... A_N} \tag{1.3}$$

$$P_{i+1} = P_i \cdot A_i \tag{1.4}$$

$$ISNR = \frac{1}{GSNR} = \sum_{i=0}^{N} \frac{P_{ni}}{P_i \cdot A_i} = \sum_{i=0}^{N} ISNR_i = \sum_{i=0}^{N} \frac{1}{GSNR_i} \tag{1.5}$$

In Equation 1.5 the GSNR is represented in a disaggregated way, by means of an additive metric (the ISNR) that can be accumulate along a path to estimate the final QoT in a DT.

The DT considered in this thesis work is Gaussian Noise in Phyton (GNPy). This tool has been developed by PLANET team of Politecnico di Torino within the context of Telecom Infra Project (TIP) [19]. GNPy is an open-source, vendor neutral QoT estimator software [20]. The TIP is one of the consortia and standardization

agencies operating with the purpose to develop open networking solutions. The TIP consortium groups most of the network operators and vendors to develop open software and hardware solutions for open networking. The TIP Open Optical and Packet Transport (OOPT) working group targets multi-layer solutions for open optical networking (OON) according to the partially disaggregated network architecture. GNPy aims to develop an open-source software model of the WDM transport layer as a DT for design, planning, and QoT estimator.

The present work builds upon the solid experience gained through past work on GNPy's DT implementation, exploiting the significant achievements of the research group responsible for its development. The project specifically concentrates on improving the mathematical models on which GNPy relies. It includes both software implementation and testing. The objective is to tackle the challenges outlined in the preceding discussion.

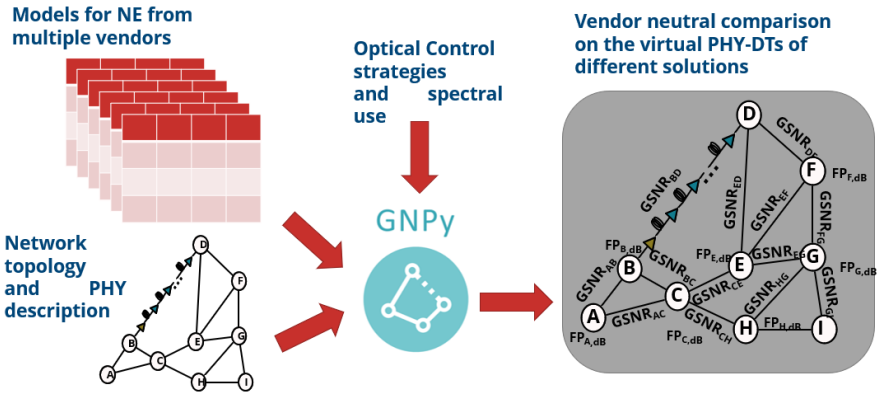

Figure 1.10: GNPy: a vendor-neutral design and planning tool

In Figure 1.10 the high level working principle of GNPy is showed. Based on inputs coming from sensors, telemetry, devices models and policies, GNPy builds a weighted graph with respect to GSNR, suited for the design and planning of the Optical Network [21].

1.4 Network as a Service

The possibilities given by a DT enables the implementation of the concept of Network as a Service (NaaS). In the past decade there has been a clear trend in applying virtualization in networking field. According to [22]: "A virtual optical network is a set of virtual optical nodes interconnected together that share a common administrative framework. Optical node virtualization is the creation of a virtual representation of an optical network node, based on an abstract model that is often achieved by partitioning or aggregation. Within a virtual optical network, virtual

connectivity (virtual link) is defined as a connection between one port of a virtual network element to a port of another virtual network element.". The virtualization paradigm allows to overcame the past custom to develop dedicated hardware to carry out networking functionalities. Virtualization based on general-purpose hardware leverages the potentiality to perform network management effectively. In such context, network resources such as bandwidth and spectral occupation can be offered and sold, leading to the NaaS implementation.

The adoption of NaaS offers several advantages that are pivotal in shaping the future of digital infrastructures. NaaS enables a more agile and cost-effective network deployment, allowing organizations to scale their infrastructure based on demand. This flexibility is crucial in the short and medium term, as it empowers businesses to adapt swiftly to changing requirements and market dynamics. Moreover, the implementation of multi-vendor infrastructure addresses interoperability challenges, fostering a competitive market environment. This not only promotes innovation but also mitigates vendor lock-in, enabling organizations to select and integrate the leading-edge solutions. In the multi-service paradigm, the ability to support diverse services within a unified framework enhances operational efficiency and resource utilization. This, in turn, has a significant impact on the short and medium-term viability of digital infrastructures, ensuring that they remain adaptable and responsive to evolving technological landscapes. Ultimately, these concepts collectively contribute to the development of innovative digital infrastructures and services, positioning organizations to meet the dynamic demands of the contemporary digital era. Their importance lies in their transformative potential, empowering businesses to stay ahead in a competitive landscape and deliver cutting-edge services to end-users.

Chapter 2

Case of Study: Polarization Dependent Loss

In this chapter the case of study of the thesis work is outlined, focusing on the OLS characterization and on the introduction of PDL phenomena.

2.1 Optical Line Systems and Switching Nodes

As mentioned in chapter 1, Optical Networks are subdivided into point-to-point connections, named OLSs, composed by a TX-RX pair and the fiber spoon and amplifiers between them. Lightpaths cross chains of OLS in order to bring information between source and destination. When two OLSs are connected a network node is created.

Figure 2.1: Optical Line System

A network node is responsible for the optical switching of the signal, which is performed thanks to ROADMs. As it has been showed in Figure 1.2, such devices rely on a specific facility, called Wavelength Selective Switch (WSS) [23]. The WSS is the main building block of optical switches and its working principle is to select a specific wavelength or a group of wavelengths conveying them towards the desired output port. Its technology is based on grating, whose diffraction effect is controlled to guide the optical signal [24].

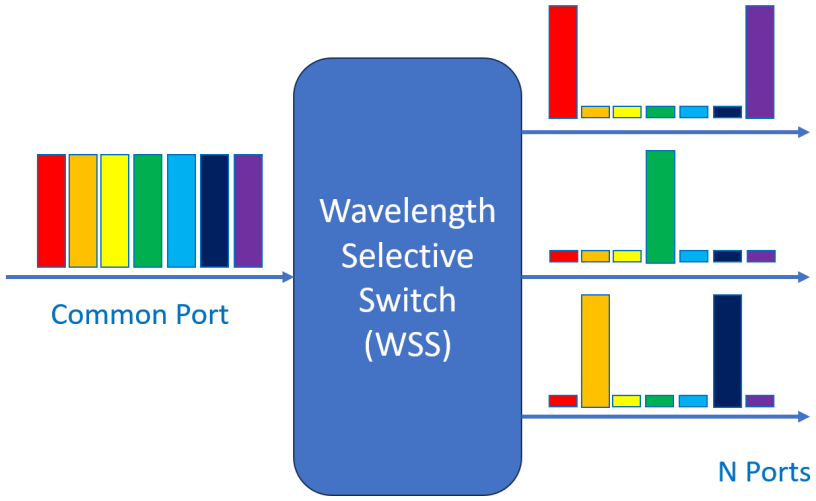

Figure 2.2: Wavelength Selective Switch

The working principle of a WSS is depicted in Figure 2.3. In the 1xN switch design, an additional lens in a Fourier transform configuration is used to perform a space-to-angle conversion in the first stage. The 1xN switch requires tilt mirrors with N different tilt angles. The design operates in the following way:

- The common input fiber enters the switch at point A, where a microlens collimates the light.
- The next lens image the collimated beam onto the diffraction grating at point C.
- The wavelength-dispersed beams then fall onto the tilt mirrors device plane at point D.
- On the tilt mirror device plane, the beams are reflected at specific tilt angles depending on the settings of the micromirrors.
- All reflected beams are focused back to point B, where the angle-to-space conversion section images the beam onto the output fiber. Each output corresponds to a specific tilt angle of the micromirrors.

One of the most common technology used in WSS to direct the light beams realizing tilt mirrors is the so-called Liquid Crystal on Silicon (LCoS) [25].

Liquid Crystal cells are able to shape the polarization of a light beam, applying a control voltage. After the Liquid Crystal cell, a polarization dependent optical

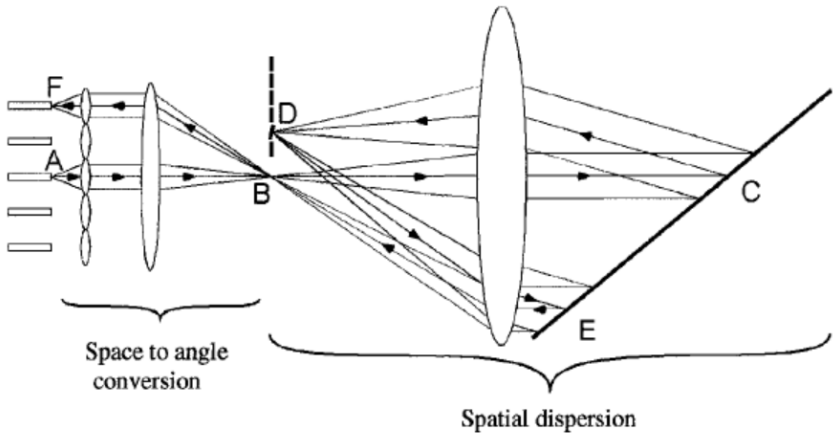

Figure 2.3: Optic system based on diffraction grating in a WSS

element (usually a Polarization Beam Splitter) is put, in order to change the beam direction based on its polarization [24]. If the input is random-polarized, it is necessary to separate it into two orthogonal polarizations. To provide attenuation, extra Liquid Crystal cells and polarization dependent elements are added to the described setup. The Liquid Crystal cell approach, combined with semiconductor technology create a high resolution, solid-state display engine. In WSS LCoS allows to create an electrically-programmable grating, suitable to realize the tils mirrors.

LCoS is particularly appealing as a switching mechanism in a WSS due to its nearly continuous addressing capability, which enables numerous new functionalities. Specifically, the bands of wavelengths that are switched together (channels) do not need to be preconfigured in the optical hardware; instead, they can be programmed into the switch through software control. Additionally, this capability allows for reconfiguring channels while the device is in operation.

LCoS technology has introduced more flexible wavelength grids, unlocking the full spectral capacity of optical fibers. The phase matrix nature of the LCoS switching element supports even more remarkable features. Common features include shaping power levels within a channel or broadcasting the optical signal to multiple ports.

LCoS-based WSS also allows dynamic control of channel center frequency and bandwidth through real-time modification of the pixel arrays via embedded software. This control can be very precise, with independent adjustment of the center frequency and either the upper or lower band edge of a channel, achieving better than 1 GHz resolution. This fine-grained control is advantageous for manufacturing, as it enables the creation of different channel plans from a single platform and allows different operating bands (such as C and L) to use an identical switch matrix.

This kind of technology, due to polarization dependent elements after Liquid Crystal cells, introduces substantial PDL, therefore an extensive study of such phenomena is pivotal in order to characterize the behaviour of a network node within the DT transmission model. It is important to underline that WSS are not the only devices introducing PDL. This happens also when Erbium Doped Fiber Amplifier (EDFA) are present along a lightpath. The contribution of EDFA in PDL penalty is not negligible at all, but its entity is small, compared to what happens in the WSS case. In this work the focus will be only on PDL induced by WSSs, leaving the discussion on EDFAs to a further work.

2.2 Polarization Dependent Loss in Wavelength Selective Switches

As already anticipated, the object of the present discussion is to delve into the PDL characterization and mathematical modeling. The PDL is a loss experienced by the optical signal which is no symmetric with respect to the state of polarization of the signal itself. This distortion, whose contribution is significant especially due to WSSs located into ROADMs, translates into a penalty applied to the signal crossing a network node. Such penalty is graphically represented in Figure 2.4, where it can be seen how a PDL device can act on a dual-polarization signal when the state of polarization is linear vertical and linear horizontal on the two polarization axis.

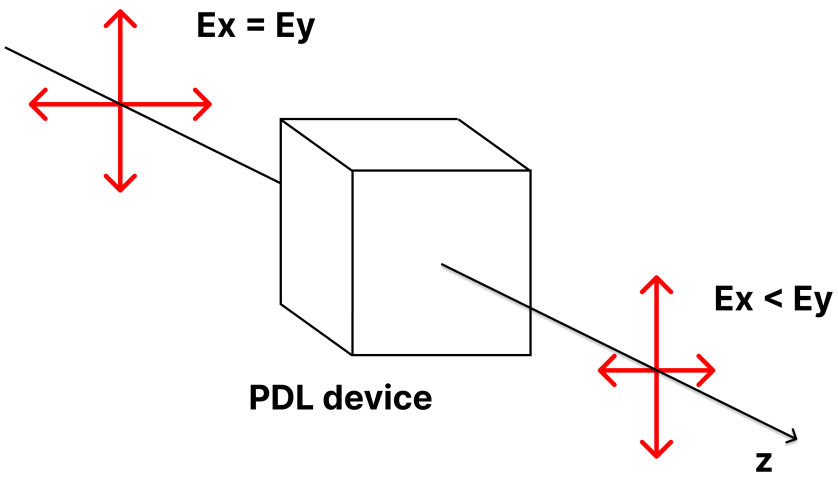

Figure 2.4: PDL

PDL has been fully analyzed for intensity-modulated channels; on the other

hand the state of the research on PDL for dual-polarized coherent channels is not at its final stage. The inclusion of PDL in the physical layer of optical networking is still not realized, and the common approach in industry is to treat it as a penalty on GSNR with a definitely conservative approach.

Indeed, the distortions caused by a sequence of PDL devices could sum up, resulting in a strong degradation of the signal. Nevertheless, as it will be clarified further on, PDL penalty is characterized by a statistical behaviour (also depending on the changes of the optical signal state of polarization along the lightpath), which leads to very frequent situations in which applying the most conservative margin on GSNR could be redundant, or at least inefficient. The statistic of PDL effect has been experimentally analyzed in [26] and [27].

As stated in chapter 1, every ROADM is composed by a set of WSSs, that are exploited to perform multiplexing tasks on WDM spectrum. The possibility of using a WSS as Multiplexer (MUX) and Demultiplexer (DEMUX) enables the add-drop functionalities and the optical switching inside a ROADM. Additionally, the WSS provides attenuation for each WDM channel.

Since manufacturing imperfection differ from a device to another and from a device port to another port of the same device, PDL changes when considering different channels on the WDM spectrum and different WSS input-output port pair. In addition, during propagation along the fibers, the optical signal experiences a random and frequency-dependent polarization rotation, which adds a further randomness to the PDL phenomena, which has to be treated stochastically.

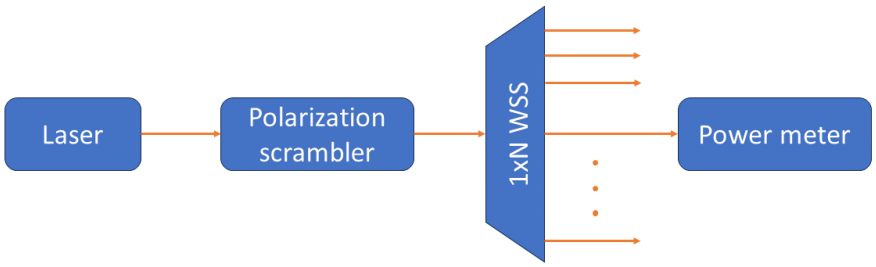

Figure 2.5: Experimental setup for PDL definition

As illustrated in [28] and considering Figure 2.5, the PDL entity introduced by

a specific input-output port pair and a specific frequency of WDM spectrum in a generic WSS is defined according to the following algorithm:

1. Select the laser frequency
2. Move the polarization. scramble to select the input signal polarization state.
3. Measure the RX optical power with the power meter.
4. Repeat from step 2. until all the possible states of polarization have been explored.
5. Let be P_{MAX} and P_{min} the maximum and minimum power values recorded during the experiment, then the PDL is then defined as:

$$PDL \triangleq 10 \log_{10} \left(\frac{P_{MAX}}{P_{min}} \right) \tag{2.1}$$

Since exploring all the possible states of polarization is not feasible in practice, this kind of measurement is often taken stopping the procedure when a sufficient portion of the Poincaré Sphere (representing all the states of polarization) has been explored, or exploiting advanced algorithms that will be illustrated in the prosecution.

2.2.1 PDL penalty

Due to its dependence from both ports and frequency, the PDL introduced by each WSS has to be treated as a random variable, especially when a full characterization of the WSS is not available. The statistical characterization of the PDL's impact on the power of both single and DP signals has been extensively studied and documented in numerous previous works in the literature [29, 30, 31, 32, 33, 34, 35, 36].

The worst-case PDL value is often provided in WSS datasheets. To simplify the theoretical discussion, a conservative SNR penalty can be considered, getting rid of the complexity of treating the PDL value as distributed in a random way. Thus, in this thesis work such value is considered as deterministic, with a certain polarization orientation. Still, the randomness of the overall phenomena is given by fiber birefringence, that leads to a random polarization rotation when the optical signal propagates. Therefore, there is a variation in time of the PDL phenomena, when several WSS are crossed, due to the birefringence. Moreover, the noise introduced at a certain point of the signal path does not experience the same PDL as the signal from TX and RX.

There is the need to define an abstraction to translate the previous concepts into a formal language. Each optical system can be divided into PDL subsystems

introducing a certain value of PDL that are described by their transfer matrices T_i, and sequences of EDFA and fibers that are responsible for the introduction of noise $\vec{N}_i$. In this context, considering n elements, the field transfer function will be described as:

$$T_{(1\to n)} = T_n \cdot T_{n-1} \cdots T_2 \cdot T_1 \tag{2.2}$$

where T_i are the PDL elements transfer matrices. The optical system is then described by its stochastic power matrix $T^{\dagger}_{(1\to n)} \cdot T_{(1\to n)}$ (the † stands for the adjoint operation, as showed in [36].

In this context, following what exposed in [28], the transmitted dual-polarization signal $\vec{S_{TX}}$ experiences the entire link PDL effect, while the noise contributions only from the point in which they are injected. Therefore to write the received signal and noise fields $\vec{S_{RX}}$ and $\vec{N_{RX}}$ it can be written:

$$\vec{S}_{\mathrm{RX}} = T_{(1\to n)}\vec{S}_{\mathrm{TX}} , \tag{2.3}$$

$$\vec{N}_{\mathrm{RX}} = \sum_{i=1}^{n} T_{(i+1\to n)}\vec{N}_i . \tag{2.4}$$

In this thesis, it is assumed that the receiver is able to recover completely the field transfer function of $\vec{S}_{\mathrm{RX}}$ so that the SNR penalty would be independent of the specific DSP implementation. Therefore, Equation 2.3 and Equation 2.4 become:

$$\vec{S}_{\mathrm{RX}} = T^{-1}_{(1\to n)}T_{(1\to n)}\vec{S}_{\mathrm{TX}} = \vec{S}_{\mathrm{TX}} , \tag{2.5}$$

$$\vec{N}_{\mathrm{RX}} = T^{-1}_{(1\to n)}\sum_{i=1}^{n} T_{(i+1\to n)}\vec{N}_i = \sum_{i=1}^{n} T^{-1}_{(1\to i)}\vec{N}_i . \tag{2.6}$$

Consequently, the $\mathrm{SNR}_{\mathrm{RX},x}$ probability distribution of a single-polarization state, x, can be derived considering the deterministic signal x-projection power, $S_{\mathrm{RX},x} = |\vec{S}_{\mathrm{RX}} \cdot \hat{x}|^2$, and the stochastic noise x-projection power, $N_{\mathrm{RX},x} = |\vec{N}_{\mathrm{RX}} \cdot \hat{x}|^2$, obtained from equation Eq. 2.6. Additionally, as the PDL of successively crossed PDL subsystems has the same effect on both the signal and the noise fields, the $\mathrm{SNR}_{\mathrm{RX},x}$ can be expressed in a disaggregated manner as the proper sum of the separate contribution of SNR degradation generated in each distinct PDL subsystem:

$$\begin{aligned}\mathrm{SNR}_{\mathrm{RX},x} &= \left(\mathrm{SNR}^{-1}_{1,x} + \cdots + \mathrm{SNR}^{-1}_{n,x}\right)^{-1} = \frac{S_{\mathrm{RX},x}}{N_{1,x} + \cdots + N_{\mathrm{n},x}} \\ &= \frac{S_{\mathrm{RX},x}}{\left|\left(T_1^{-1}\vec{N}_1\right)\cdot\hat{x}\right|^2 + \cdots + \left|\left(T^{-1}_{(1\to n)}\vec{N}_{\mathrm{n}}\right)\cdot\hat{x}\right|^2}\end{aligned} \tag{2.7}$$

Given Equation 2.7, it is clear that finding an effective way to describe how PDL acts on noise is pivotal in retrieving the SNR in a disaggregated way. The following discussion aims to develop a mathematical tool able to model in n accurate way the distribution of noise power among the polarization axis, when crossing PDL elements such as WSSs.

Chapter 3

Theoretical Background

In this chapter the mathematical tools necessary to cope with polarization of electromagnetic fields are recalled, with a special attention to Jones matrices theory. This step is pivotal in order to introduce the mathematical derivation of the proposed PDL analytical model, which aims to enhance GNPy DT transmission model. The tools illustrated in the final part of this chapter are based on previous work of PLANET team, in continuity with the objective to develop the open and disaggregated paradigm in optical networking.

3.1 Fundamentals of Polarization

The "state of polarization" of light is one of the three fundamental parameters that characterize a light signal, along with frequency and wave vector. The "state of polarization" is a property that light exhibits both in its electromagnetic (wave) representation and in its intensity representation (number of photons). It is, therefore, a fundamental characteristic of light and its basic constituents: photons. It is important to know the state of polarization and to be able to estimate its evolution because many optical devices and components are "polarization-sensitive," meaning their behavior depends on the polarization state of the incoming light. Generally, the polarization state of a light signal changes during its propagation when it encounters an anisotropic medium, that is, a medium that has a different refractive index in different spatial directions. A typical example of an anisotropic medium is optical fiber propagation, where a combination of mechanical and thermal causes produces anisotropy in the glass material that constitutes the optical fiber. Therefore, it can be important to have methods that allow predicting the evolution of the polarization state of an incoming light signal in the optical fiber or another anisotropic material. The content of this section summarizes a commonly developed methodology for this purpose: the Jones vector and matrix approach. All the

discussion is taken from [37], which covers the topic much more widely.

3.1.1 Jones vectors

One of the most commonly used representations to describe the state of polarization of light is known as the Jones Representation. It originates from a description of the electromagnetic field decomposed into two components along the Cartesian axes x and y.

$$E_x = E_{x_0} e^{-i(\omega t - kz - \delta_x)} \tag{3.1}$$

$$E_y = E_{y_0} e^{-i(\omega t - kz - \delta_y)} \tag{3.2}$$

That can be rewritten considering only the terms that have effect on the state of polarization:

$$\begin{bmatrix} E_x \\ E_y \end{bmatrix} = \begin{bmatrix} E_{x_0} e^{i\delta_x} \\ E_{y_0} e^{i\delta_y} \end{bmatrix} \tag{3.3}$$

The Equation 3.3 is the so-called "Jones vector". It can be shown that, through an opportune choice of the 4 parameters:

$$E_{x_0} \text{ x component amplitude} \tag{3.4}$$

$$E_{y_0} \text{ y component amplitude} \tag{3.5}$$

$$\delta_x \text{ x component phase delay} \tag{3.6}$$

$$\delta_y \text{ y component phase delay} \tag{3.7}$$

It is possible to describe any state of polarization of coherent light. Jones representation is advantageous since it is simply and accurate to describe operations on polarization that involve a sequence of birefringent elements.

Optical field is not a quantity accessible to the measure, therefore often it is useful to compute the intensity I in order to sense the polarization properties:

$$I = E_x \cdot E_x^* + E_y \cdot E_y^* \tag{3.8}$$

Namely:

$$I = \begin{bmatrix} E_x^* & E_y^* \end{bmatrix} \cdot \begin{bmatrix} E_x \\ E_y \end{bmatrix} \tag{3.9}$$

In Equation 3.9, the first vector is also known as "transpose conjugate" vector. The generic Jones vector is represented also with the notation:

$$\begin{bmatrix} E_{x_0} e^{i\delta_x} \\ E_{y_0} e^{i\delta_y} \end{bmatrix} = \left| \begin{matrix} E_{x_0} e^{i\delta_x} \\ E_{y_0} e^{i\delta_y} \end{matrix} \right\rangle = \left| E_x \quad E_y \right\rangle \tag{3.10}$$

With this alternative notation, the transpose conjugate vector is represented as:

$$\begin{bmatrix} E_x^* & E_y^* \end{bmatrix} = \begin{vmatrix} E_x & E_y \end{vmatrix} \tag{3.11}$$

So the intensity of a generic state of polarization is given by:

$$I = \begin{vmatrix} E_x & E_y \end{vmatrix} \begin{vmatrix} E_x & E_y \end{vmatrix} \tag{3.12}$$

The principal 6 stated of polarization are obtained by assigning specific values to the 4 main parameters:

$$H = \begin{bmatrix} 1 \\ 0 \end{bmatrix} \text{ Linear Horizontal} \tag{3.13}$$

$$V = \begin{bmatrix} 0 \\ 1 \end{bmatrix} \text{ Linear Vertical} \tag{3.14}$$

$$Q = \frac{1}{\sqrt{2}} \begin{bmatrix} 1 \\ 1 \end{bmatrix} \text{ Linear } 45° \tag{3.15}$$

$$-Q = \frac{1}{\sqrt{2}} \begin{bmatrix} 1 \\ -1 \end{bmatrix} \text{ Linear -}45° \tag{3.16}$$

$$R = \frac{1}{\sqrt{2}} \begin{bmatrix} 1 \\ i \end{bmatrix} \text{ Right-hand Circular} \tag{3.17}$$

$$L = \frac{1}{\sqrt{2}} \begin{bmatrix} 1 \\ -i \end{bmatrix} \text{ Left-hand Circular} \tag{3.18}$$

It interesting to note that all the pairs of state of polarization described from Equation 3.13 to Equation 3.18 are orthogonal, namely:

$$I = \begin{vmatrix} E_{x_1} & E_{y_1} \end{vmatrix} \begin{vmatrix} E_{x_2} & E_{y_2} \end{vmatrix} = 0 \tag{3.19}$$

3.1.2 Jones operators

The evolution of the state of polarization of an optical signal is modeled with the introduction of matrices that "operate" on Jones vectors. This formalism allows to compute the input and output state of polarization. In general it is possible to write:

$$\begin{vmatrix} E_{x_{out}} \\ E_{y_{out}} \end{vmatrix} = \begin{bmatrix} j_{xx} & j_{xy} \\ j_{yx} & j_{yy} \end{bmatrix} \begin{vmatrix} E_{x_{in}} \\ E_{y_{in}} \end{vmatrix} \tag{3.20}$$

Where j_{xx}, j_{xy}, j_{yx}, $j_{yy} \in \mathbb{C}$.

At the output, the intensity of the optical signal will be evaluated by:

$$I_{out} = \begin{vmatrix} E_{x_{out}} & E_{y_{out}} \end{vmatrix} \begin{vmatrix} E_{x_{out}} & E_{y_{out}} \end{vmatrix} \tag{3.21}$$

If the Jones operator is represented as:

$$J = \begin{bmatrix} j_{xx} & j_{xy} \\ j_{yx} & j_{yy} \end{bmatrix} \tag{3.22}$$

Then, if a sequence of n operation on polarization are performed, the scheme in Equation 3.20 can be applied sequentially, obtaining:

$$\begin{vmatrix} E_{x_{out}} \\ E_{y_{out}} \end{vmatrix} = J_n \cdots J_2 \cdot J_1 \cdot \begin{vmatrix} E_{x_{in}} \\ E_{y_{in}} \end{vmatrix} \tag{3.23}$$

The Jones operator that is useful for the present discussion is the polarizer, which is described by the following expressions:

$$E_{x_{out}} = l_x \cdot E_{x_{in}} \tag{3.24}$$

$$E_{y_{out}} = l_y \cdot E_{y_{in}} \tag{3.25}$$

where $0 \leq p_{x,y} \leq 1$. For complete transmission $p_{x,y} = 1$, and for complete attenuation $p_{x,y} = 0$. In terms of the Jones vector, Equation 3.24 and Equation 3.25 can be written as:

$$\begin{vmatrix} E_{x_{out}} \\ E_{y_{out}} \end{vmatrix} = \begin{bmatrix} p_x & 0 \\ 0 & p_y \end{bmatrix} \cdot \begin{vmatrix} E_{x_{in}} \\ E_{y_{in}} \end{vmatrix} \tag{3.26}$$

This operator is suited to describe PDL, since it can express the loss experienced by the optical signal on two different components. For instance, looking at Figure 2.4, the signal is horizontally and vertically polarized, therefore the loss on x-axis can be represented as an opportune coefficient l_x in the polarizer Jones operator.

The PDL in general is not aligned to x or y axis, therefore the next step is to represent it with respect to a rotation angle that, in general, will be random. The aim of section 3.2 is to adapt what recalled in this section about Jones theory to the case of study of PDL.

3.2 Definitions

In order to represent the geometrical rotations of Jones vectors and operators, the following real rotation matrix is adopted:

$$R(\theta) = \begin{bmatrix} \cos\theta & -\sin\theta \\ \sin\theta & \cos\theta \end{bmatrix} \tag{3.27}$$

When dealing with optical fibers, their birefringent behaviour is generally modelled through a complex rotation matrix:

$$R(\theta, \phi) = \begin{bmatrix} \cos\theta e^{i\phi} & -\sin\theta e^{i\phi} \\ \sin\theta e^{-i\phi} & \cos\theta e^{-i\phi} \end{bmatrix} \tag{3.28}$$

Rotation matrices are applied before and after a Jones operator, so that, if a geometric rotation has to be represented for the generic operator J, the procedure to follow is:

$$J(\theta) = R(\theta)^{\dagger} \cdot J \cdot R(\theta) = R(\theta)^{T} \cdot J \cdot R(\theta) \tag{3.29}$$

Where the transpose-conjugate operation † is equivalent to the matrix transposition, since $R(\theta) \in \mathbb{R}$.

When dealing with diagonal Jones operators, complex rotations are equivalent to real rotations, as it is showed in the following proof:

$$\begin{aligned} J(\theta) &= R(\theta,\phi)^{\dagger} \cdot J_{diag} \cdot R(\theta,\phi) \\ &= \begin{bmatrix} \cos\theta e^{-i\phi} & \sin\theta e^{i\phi} \\ -\sin\theta e^{-i\phi} & \cos\theta e^{i\phi} \end{bmatrix} \begin{bmatrix} j_{11} & 0 \\ 0 & j_{22} \end{bmatrix} \begin{bmatrix} \cos\theta e^{i\phi} & -\sin\theta e^{i\phi} \\ \sin\theta e^{-i\phi} & \cos\theta e^{-i\phi} \end{bmatrix} \\ &= \begin{bmatrix} j_{11}\cos^2\theta + j_{22}\sin^2\theta & (j_{22}-j_{11})\sin\theta\cos\theta \\ (j_{22}-j_{11})\sin\theta\cos\theta & j_{11}\sin^2\theta + j_{22}\cos^2\theta \end{bmatrix} \\ &= R(\theta)^{T} \cdot J_{diag} \cdot R(\theta) \quad \square \end{aligned} \tag{3.30}$$

The angle θ in the framework that is going to be developed models the rotation of alignment both between the transmitted signal state of polarization and the main polarization axes of a general PDL element and the alignment between the main axes of two PDL elements. For this reason it is a random variable uniformly distributed as:

$$\theta \sim \mathcal{U}([0, 2\pi]) \tag{3.31}$$

An useful property of rotation matrices, when they are real follows:

$$R(\theta)^{\dagger} = R(\theta)^{T} = R(\theta)^{-1} \tag{3.32}$$

In the following, since in general Jones matrices are complex, the preferred notation will be the use of †, namely the transpose conjugate operation.

3.2.1 PDL element field matrix description

The starting point to define the Jones operator of a PDL element, also called "field matrix" is the polarizer defined in Equation 3.26. To represent geometrical rotation and fiber birefringence, a rotation is applied to it, because in general PDL is not aligned to the main polarization axis of the incoming signal. The rotated polarizer expression is then:

$$\begin{aligned} Pol(\theta) &= \begin{bmatrix} \cos\theta & \sin\theta \\ -\sin\theta & \cos\theta \end{bmatrix} \begin{bmatrix} \sqrt{l_x} & 0 \\ 0 & \sqrt{l_y} \end{bmatrix} \begin{bmatrix} \cos\theta & -\sin\theta \\ \sin\theta & \cos\theta \end{bmatrix} \\ &= R(\theta)^{\dagger} \cdot P \cdot R(\theta) \end{aligned} \tag{3.33}$$

Differently from Equation 3.26, here $p_x = \sqrt{l_x}$ and $p_y = \sqrt{l_y}$, because l_x and l_y represent a loss in term of power, while p_x and p_y are losses in field domain, therefore the square root is needed to link them. If $\sqrt{l_x}+\sqrt{l_y} = 1$ then the polarizer is ideal, therefore all the power of the incoming signal crossing the polarizer is conserved, even if switched among the two polarization axis. When $\sqrt{l_x} + \sqrt{l_y} < 1$ a loss of power is experienced by the signal, which is the case when dealing with PDL.

Considering an alternative definition of PDL than the one provided in Equation 2.1:

$$pdl = \frac{l_M}{l_m} \tag{3.34}$$

Where l_M and l_m are respectively the maximum and the minimum loss of power experienced for all the possible polarization states of the incoming signal. Then, it is possible to assign $l_x = l_M$ and $l_y = l_m$ and, following the key assumption:

$$l_M + l_m = 2L \tag{3.35}$$

Where L is the total loss, the two losses can be written in term of PDL as follows:

$$l_x = l_M = L * \frac{2 * pdl}{pdl + 1} \tag{3.36}$$

$$l_y = l_m = L * \frac{2}{pdl + 1} \tag{3.37}$$

From this point on, the field matrix will be called T, and it can be rewritten as:

$$\begin{aligned} T &= \begin{bmatrix} \cos\theta & \sin\theta \\ -\sin\theta & \cos\theta \end{bmatrix} \begin{bmatrix} \sqrt{l_x} & 0 \\ 0 & \sqrt{l_y} \end{bmatrix} \begin{bmatrix} \cos\theta & -\sin\theta \\ \sin\theta & \cos\theta \end{bmatrix} \\ &= \begin{bmatrix} \sqrt{l_x}\cos^2\theta + \sqrt{l_y}\sin^2\theta & (\sqrt{l_y} - \sqrt{l_x})\sin\theta\cos\theta \\ (\sqrt{l_y} - \sqrt{l_x})\sin\theta\cos\theta & \sqrt{l_x}\sin^2\theta + \sqrt{l_y}\cos^2\theta \end{bmatrix} \end{aligned} \tag{3.38}$$

The inverse of T is easy to be computed, since the focus is on simple 2x2 matrices. As anticipated in subsection 2.2.1 DSP is responsible to invert the distortion on the transmitted signal due to PDL, therefore is it useful to compute T^{-1} for the purpose of this work:

$$\begin{aligned} T^{-1} &= \frac{1}{\sqrt{l_x l_y}} \begin{bmatrix} \cos\theta & \sin\theta \\ -\sin\theta & \cos\theta \end{bmatrix} \begin{bmatrix} \sqrt{l_y} & 0 \\ 0 & \sqrt{l_x} \end{bmatrix} \begin{bmatrix} \cos\theta & -\sin\theta \\ \sin\theta & \cos\theta \end{bmatrix} \\ &= \frac{1}{\sqrt{l_x l_y}} \begin{bmatrix} \sqrt{l_y}\cos^2\theta + \sqrt{l_x}\sin^2\theta & (\sqrt{l_x} - \sqrt{l_y})\sin\theta\cos\theta \\ (\sqrt{l_x} - \sqrt{l_y})\sin\theta\cos\theta & \sqrt{l_y}\sin^2\theta + \sqrt{l_x}\cos^2\theta \end{bmatrix} \end{aligned} \tag{3.39}$$

Starting from T, the mot important tool for the mathematical model developed in this work is the power transfer matrix, which is well-known in literature [36]. The power transfer matrix describes how the intensity, and consequently the power, distributes among the two polarization axis when a signal crosses an element introducing PDL. Commonly power transfer matrix is defined as $T^\dagger T$. Its expression follows:

$$\begin{aligned} T^\dagger T &= R(\theta)^\dagger \begin{bmatrix} \sqrt{l_x} & 0 \\ 0 & \sqrt{l_y} \end{bmatrix} R(\theta) R(\theta)^\dagger \begin{bmatrix} \sqrt{l_x} & 0 \\ 0 & \sqrt{l_y} \end{bmatrix} R(\theta) \\ &= R(\theta)^\dagger \begin{bmatrix} l_x & 0 \\ 0 & l_y \end{bmatrix} R(\theta) \\ &= \begin{bmatrix} l_x cos^2\theta + l_y sin^2\theta & (l_y - l_x) cos\theta sin\theta \\ (l_y - l_x) cos\theta sin\theta & l_x sin^2\theta + l_y cos^2\theta \end{bmatrix} \end{aligned} \tag{3.40}$$

Significantly, the expression of the power transfer matrix is the same as T, with the only difference that on the main diagonal, square roots are not present. This comes from its structure and from the rotation matrix properties.

The power transfer matrix is the key element of the mathematical model of PDL because the objective is to represent how the noise power behaves crossing PDL elements. Some issues have to be taken into account when passing from fields to powers. The space of Jones vectors and matrices is a vector space, while power transfer matrices and power vectors are not, due to their quadratic definition. Therefore, it is important to outline the parallelism of these two approaches, but considering also that they are inherently different.

The power transfer matrix paradigm does not offer many advantages when describing the transmitted signal. Its power shows up when considering noise, as it will be clear in the prosecution. This is important when assuming the presence of DSP at the RX that is able to fully recover the information of the signal inverting also the PDL distortions acting on it. In this case only noise will be affected by PDL in a way that DSP is not able to fully recover, since noise is additively injected along the signal lightpath and experiences different PDL distortion than the signal. Noise is difficult to be represented through Jones formalism, since its components are random. Usually it is better to treat it from its power perspective. When noise power evolution along the path is mathematically well described, it is easy to obtain a penalty in term of SNR to represent the PDL impairment.

3.2.2 Transmitted signal and noise field description

In this formalism, the transmitted signal for a single frequency channel, which is fully recovered by the DSP, is not modulated, for simplicity. Its Jones vector is

defined as:

$$\vec{s} = \begin{bmatrix} \frac{1}{\sqrt{2}} \\ \frac{1}{\sqrt{2}} \end{bmatrix} \tag{3.41}$$

So that its intensity is normalized to 1, namely:

$$I(\vec{s}) = \vec{s}^{\dagger} \cdot \vec{s} = 1 \tag{3.42}$$

Given a noise signal of total power equal to N, that is injected in the lightpath, we define its Jones field vector as:

$$\vec{n} \quad = \quad \begin{bmatrix} n_x \\ n_y \end{bmatrix} \quad n_x, n_y \sim \mathcal{G}\left(0, \frac{N}{2}\right) \tag{3.43}$$

Where n_x and n_y have a gaussian Probability Density Function (PDF) and they have the same variance since PDL distortion has not been applied yet to the noise. A general noise vector od power N is defined as:

$$\vec{n}(\sigma_1, \sigma_2) \quad = \quad \begin{bmatrix} n'_x \\ n'_y \end{bmatrix} \quad n'_x \sim \mathcal{G}(0, \sigma_1) \quad n'_y \sim \mathcal{G}(0, \sigma_2) \quad \sigma_1 + \sigma_2 = N \tag{3.44}$$

Properties:

$$\mathbb{E}[\vec{n}] \quad = \quad \mathbb{E}\left[\begin{bmatrix} n_x \\ n_y \end{bmatrix}\right] = \begin{bmatrix} 0 \\ 0 \end{bmatrix} \tag{3.45}$$

$$Var(\vec{n}) \quad = \quad \mathbb{E}[\vec{n} \cdot \vec{n}^T] = \mathbb{E}\left[\begin{bmatrix} n_x \\ n_y \end{bmatrix} \begin{bmatrix} n_x & n_y \end{bmatrix}\right] = \begin{bmatrix} \frac{N}{2} & 0 \\ 0 & \frac{N}{2} \end{bmatrix} \tag{3.46}$$

When considering Jones vectors having random variables as their components, the intensity computation must involve also the expectation. Here it is called P to distinguish it from the simple intensity I defined in Equation 3.9.

$$P(\vec{n}) \quad = \quad \mathbb{E}[\vec{n}^{\dagger} \cdot \vec{n}] = \mathbb{E}\left[\begin{bmatrix} n_x* & n_y* \end{bmatrix} \begin{bmatrix} n_x \\ n_y \end{bmatrix}\right] = \mathbb{E}[n_x^2 + n_y^2] = N \tag{3.47}$$

The power vector that describes the case in which noise power is equally distributed among the two polarizations, when dealing with power transfer matrices is defined, as:

$$\vec{p}_n = \begin{bmatrix} Var(n_x) \\ Var(n_y) \end{bmatrix} = \begin{bmatrix} \frac{N}{2} \\ \frac{N}{2} \end{bmatrix} \tag{3.48}$$

Then, if it is needed to compute the noise total intensity from the power vector it is simply necessary to sum the two components:

$$\mathcal{P}[\vec{p}_n] = \mathcal{P}(\vec{n}) = Var(n_x) + Var(n_y) = \frac{N}{2} + \frac{N}{2} = N \tag{3.49}$$

In general, starting from the power vector $\vec{p}$, its intensity is computed as follows:

$$\vec{p} = \begin{bmatrix} p_x \\ p_y \end{bmatrix} \tag{3.50}$$

$$\mathcal{P}[\vec{p}] = p_x + p_y \tag{3.51}$$

When dealing with power transfer matrices and uncorrelated random variables, often a special type of product between a vector and a matrix is found to be useful. This "special product" between a matrix and a vector takes only the matrix main diagonal terms to be multiplied with the vector terms:

$$A = \begin{bmatrix} a_{11} & a_{12} \\ a_{21} & a_{22} \end{bmatrix} \tag{3.52}$$

$$\vec{v} = \begin{bmatrix} v_1 \\ v_2 \end{bmatrix} \tag{3.53}$$

$$A \odot \vec{v} = \begin{bmatrix} a_{11} \cdot v_1 \\ a_{22} \cdot v_2 \end{bmatrix} \tag{3.54}$$

3.3 PDL mathematical model derivation

Starting from section 3.2, in this part the chosen mathematical model to manage PDL impairments is developed. First of all the single PDL device is analyzed, modelling the evolution of noise power. Then the model is extended to a cascade of PDL devices. Finally, a disaggregated version of the model is considered, in view of a possible implementation on GNPy DT.

3.3.1 Single PDL device

What is showed in this section is that, given the field matrix T of a single PDL device (such as a WSS) and the noise vector $\vec{n}$ of power N that is injected before it, it is possible to compute the output noise power in the two polarizations from the power transfer matrix $T^\dagger T$, through the previously-called "special product" $\odot$. Therefore, it has to be proven that:

$$P(T \cdot \vec{n}) = \mathcal{P}[T^\dagger T \odot \vec{p}_n] \tag{3.55}$$

First of all it is possible to start computing the right member of Equation 3.55, since it is straightforward to evaluate it. Looking at Equation 3.40 and Equation 3.48, the result of the special product is:

$$\begin{aligned} T^{\dagger}T \odot \vec{p}_n &= \begin{bmatrix} l_x cos^2\theta + l_y sin^2\theta & (l_y - l_x)cos\theta sin\theta \\ (l_y - l_x)cos\theta sin\theta & l_x sin\theta + l_y cos^2\theta \end{bmatrix} \odot \begin{bmatrix} \frac{N}{2} \\ \frac{N}{2} \end{bmatrix} \\ &= \begin{bmatrix} \frac{N}{2}(l_x cos^2\theta + l_y sin\theta^2) \\ \frac{N}{2}(l_x sin^2\theta + l_y cos^2\theta) \end{bmatrix} \end{aligned} \tag{3.56}$$

Therefore, the total power is:

$$\mathcal{P}[T^{\dagger}T \odot \vec{p}_n] = \frac{N}{2}(l_x + l_y) \tag{3.57}$$

Now the left-member of Equation 3.55 has to be evaluated:

$$\begin{aligned} T \cdot \vec{n} &= \begin{bmatrix} \sqrt{l_x}\cos^2\theta + \sqrt{l_y}\sin^2\theta & (\sqrt{l_y} - \sqrt{l_x})\sin\theta\cos\theta \\ (\sqrt{l_y} - \sqrt{l_x})\sin\theta\cos\theta & \sqrt{l_x}\sin^2\theta + \sqrt{l_y}\cos^2\theta \end{bmatrix} \cdot \begin{bmatrix} n_x \\ n_y \end{bmatrix} \\ &= \begin{bmatrix} n_x(\sqrt{l_x}\cos^2\theta + \sqrt{l_y}\sin^2\theta) + n_y((\sqrt{l_y} - \sqrt{l_x})\sin\theta\cos\theta) \\ n_x((\sqrt{l_y} - \sqrt{l_x})\sin\theta\cos\theta) + n_y(\sqrt{l_x}\sin^2\theta + \sqrt{l_y}\cos^2\theta) \end{bmatrix} \\ &= \begin{bmatrix} n_{outx} \\ n_{outy} \end{bmatrix} \end{aligned} \tag{3.58}$$

Then, to obtain the total power the sum of the variance of the two components in Equation 3.58 has to be computed, according to the property showed in Equation 3.49:

$$P(T \cdot \vec{n}) = Var(n_{outx}) + Var(n_{outy}) \tag{3.59}$$

The two variances are now compute independently, based on the components of Equation 3.58.

$$\begin{aligned} Var(n_{outx}) &= \mathbb{E}[n_{outx}^2] \\ &= \mathbb{E}[(n_x(\sqrt{l_x}\cos^2\theta + \sqrt{l_y}\sin^2\theta) + \\ &\quad + n_y((\sqrt{l_y} - \sqrt{l_x})\sin\theta\cos\theta))^2] \\ &= \mathbb{E}[n_x^2(\sqrt{l_x}\cos^2\theta + \sqrt{l_y}\sin^2\theta)^2 + \\ &\quad + n_y^2(\sqrt{l_y} - \sqrt{l_x})^2\sin^2\theta\cos^2\theta + \\ &\quad + 2n_x n_y(\sqrt{l_x}\cos^2\theta + \sqrt{l_y}\sin^2\theta)(\sqrt{l_y} - \sqrt{l_x})\sin\theta\cos\theta] \end{aligned} \tag{3.60}$$

Since $n_x \perp\!\!\!\perp n_y$, the term in passage 3.60 is equal to zero when applying the expectation:

$$\begin{aligned} Var(n_{outx}) &= \frac{N}{2}[(\sqrt{l_x}\cos^2\theta + \sqrt{l_y}\sin^2\theta)^2 + \\ &\quad +(\sqrt{l_y} - \sqrt{l_x})^2\sin^2\theta\cos^2\theta] \\ &= \frac{N}{2}[l_x\cos^4\theta + l_y\sin^4\theta + 2\sqrt{l_x l_y}\sin^2\theta\cos^2\theta + \\ &\quad +l_x\sin^2\theta\cos^2\theta + l_y\sin^2\theta\cos^2\theta - 2\sqrt{l_x l_y}\sin^2\theta\cos^2\theta] \\ &= \frac{N}{2}[l_x\cos^4\theta + l_y\sin^4\theta + \\ &\quad +l_x\sin^2\theta\cos^2\theta + l_y\sin^2\theta\cos^2\theta] \\ &= \frac{N}{2}[l_x\cos^2\theta + l_y\sin^2\theta] \end{aligned} \tag{3.61}$$

Similarly, focusing on the y-polarization, a symmetric result is obtained in carrying on the same computations to retrieve $Var(n_{outy})$:

$$Var(n_{outy}) = \frac{N}{2}[l_x\sin^2\theta + l_y\cos^2\theta] \tag{3.62}$$

Then, exploiting what obtained for $Var(n_{outx})$ and $Var(n_{outy})$, starting from Equation 3.59, it can be concluded:

$$P(T\cdot\vec{n}) = Var(n_{outx}) + Var(n_{outy}) = \frac{N}{2}(l_x + l_y) = \mathcal{P}[T^\dagger T \odot \vec{p}_n] \quad \square \tag{3.63}$$

What has been proved is that the power transfer matrix paradigm is able to describe effectively the total noise power evolution when crossing a PDL element, but more conclusions can be extrapolate. Observing the passages carried on in the previous derivation, it is possible to see that the "special product" gives in output two components that describe the amount of noise power that is in each polarization axis. This is confirmed by comparing the two components obtained from the "special product" in Equation 3.56 and the values of the power of the two noise field components, computed in Equation 3.61 and Equation 3.62. If these two components are summed up, the total noise power is correctly obtained. Therefore, it holds that:

$$|T\vec{n}\cdot\hat{x}|^2 = T^\dagger T \odot \vec{p}_n \cdot \hat{x} \tag{3.64}$$

$$|T\vec{n}\cdot\hat{y}|^2 = T^\dagger T \odot \vec{p}_n \cdot \hat{y} \tag{3.65}$$

In conclusion, the power transfer matrix paradigm, based on "special product" allows to compute easily with simple operations the evolution of noise power among the two polarization axis when crossing a PDL device. This result leads to an effective, fast and disaggregated computation of SNR that can be implemented in a DT such as GNPy.

3.3.2 Cascade of PDL devices

The first extension to be made is when noise introduced at a certain point of the link crosses a sequence of M PDL devices. This case is exemplified in Figure 3.1.

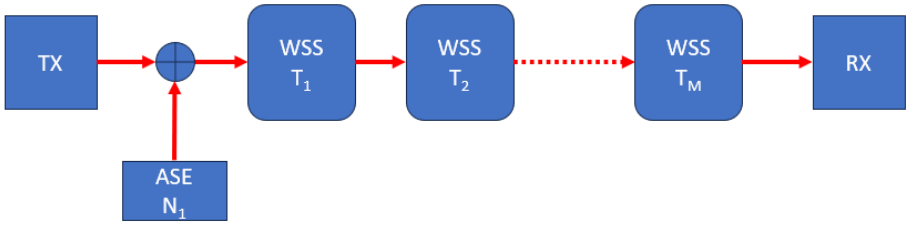

Figure 3.1: Single noise propagation through PDL devices block diagram

To obtain the noise power distributed among the two main polarization axes, through the model derived in subsection 3.3.1, it is sufficient to compute the Jones operator of the entire cascade, from which the total power transfer matrix of the cascade will be obtained. To express the product of a sequence of Jones operator, the formalism anticipated in Equation 2.2 is adopted for the derivation.

$$T_{TOT} = T_M \cdots T_2 \cdot T_1 = T_{(1 \to M)} \tag{3.66}$$

$$\vec{p}_{n,out} = \begin{bmatrix} p_{x,out} \\ p_{y,out} \end{bmatrix} = (T_{TOT})^{\dagger} T_{TOT} \odot \vec{p}_n \tag{3.67}$$

This comes from the properties of Jones operators showed in Equation 3.23, then when having obtained the total Jones operator, the noise power components computations follows from the proof of Equation 3.55.

In general, noise can be introduced in more than one point of a lightpath, therefore it is necessary to extend the model to the case in which there are more than one noise contributions added between the PDL devices. Moreover, the case of interest of this work is when DSP recovers the information signal at the end of the path, applying a correction in term of PDL to the TX optical signal, that is the same applied to all the noise contribution, independently from their point of injection. Such premises are summarized by the block diagram in Figure 3.2.

The key assumption to be made is that the superposition principle holds for the effect of multiple independent noise sources, so that the total noise power is the sum of each single noise contribution after propagation across the PDL devices. According to this assumption, it is just necessary to derive the expression of the accumulated Jones operator that acts on the generic i-th noise field $\vec{n}_i$ injected along the lightpath. Then the power transfer matrix of the i-th noise contribution

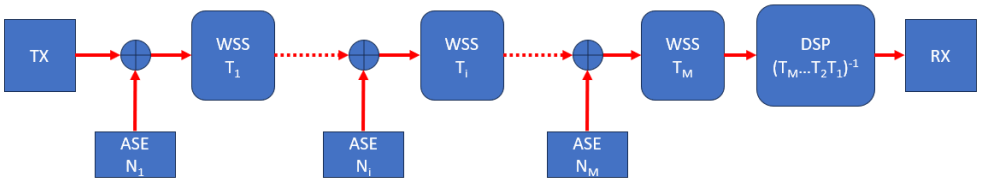

Figure 3.2: Multiple noise propagation through PDL devices and DSP action block diagram

will be used to compute the output noise power vector $\vec{p}_{n,out,i}$ from the input power vector $\vec{p}_{n,i}$ for that noise source, which will be summed with all the other noise contributions output power vectors.

The Jones operator that acts on a generic noise field injected in the position "i" of the lightpath is expressed as the product between the Jones operator of the PDL elements through which the noise field propagates T_{PROP} and the Jones operator applied by DSP T_{DSP} that inverts the distortion that the TX signal experiences along the entire path from T_1 to T_M:

$$T_{n,i} = T_{DSP} \cdot T_{PROP} = T^{-1}_{(1\to M)} \cdot T_{(i\to M)} = T^{-1}_{(1\to i-1)} \tag{3.68}$$

If the first noise contribution is considered, the DSP eliminates all the PDL impairment as it does for the TX signal, therefore the Jones operator is the identity matrix:

$$T_{n,1} = T^{-1}_{(1\to 0)} = T_{(1\to 0)} = \begin{bmatrix} 1 & 0 \\ 0 & 1 \end{bmatrix} \tag{3.69}$$

The output power vector of the i-th noise contribution is then computed starting from the power transfer matrix obtained from $T_{n,i}$, through the "special product":

$$\vec{p}_{n,out,i} = T^{\dagger}_{n,i} T_{n,i} \odot \vec{p}_{n,i} \tag{3.70}$$

All the noise contribution from 1 to M have to be summed up to obtain the total amount of noise power distributed in the two main polarization axes:

$$\begin{aligned} \vec{p}_{n,TOT} &= \sum_{i=1}^{M} \vec{p}_{n,out,i} = \sum_{i=1}^{M} T^{\dagger}_{n,i} T_{n,i} \odot \vec{p}_{n,i} \\ &= \sum_{i=1}^{M} \left(T^{-1}_{(1\to i-1)}\right)^{\dagger} T^{-1}_{(1\to i-1)} \odot \vec{p}_{n,i} \end{aligned} \tag{3.71}$$

Focusing on the transmitted optical signal, it is easy to show that its power is conserved due to the DSP action:

$$I(\vec{s}_{out}) = I\left(T_{DSP} \cdot T_{TOT} \cdot \vec{s}\right) = I\left(T^{-1}_{(1\to M)} \cdot T_{(1\to M)} \cdot \vec{s}\right) = I(\vec{s}) = 1 \tag{3.72}$$

After computing the power of signal and noise, it is possible to express the total SNR of the system:

$$SNR_{RX} = \frac{I(\vec{s}_{out})}{\mathcal{P}[\vec{p}_{n,TOT}]} = \frac{1}{\mathcal{P}\left(\sum_{i=1}^{M}\left(T^{-1}_{(1\to i-1)}\right)^{\dagger} T^{-1}_{(1\to i-1)} \odot \vec{p}_{n,i}\right)} \tag{3.73}$$

It is also possible to compute separately the SNR for both the main polarization axis, thanks to the structure of power vectors that allows to separate the total power in two components relative to the x or y polarization:

$$SNR_{RX,x} = \frac{|\vec{s}_{out} \cdot \hat{x}|^2}{\vec{p}_{n,TOT} \cdot \hat{x}} = \frac{1}{2}\frac{1}{\sum_{i=1}^{M}\left(T^{-1}_{(1\to i-1)}\right)^{\dagger} T^{-1}_{(1\to i-1)} \odot \vec{p}_{n,i} \cdot \hat{x}} \tag{3.74}$$

$$SNR_{RX,y} = \frac{|\vec{s}_{out} \cdot \hat{y}|^2}{\vec{p}_{n,TOT} \cdot \hat{y}} = \frac{1}{2}\frac{1}{\sum_{i=1}^{M}\left(T^{-1}_{(1\to i-1)}\right)^{\dagger} T^{-1}_{(1\to i-1)} \odot \vec{p}_{n,i} \cdot \hat{y}} \tag{3.75}$$

After computing the total SNR it is necessary, in view of the model inclusion in GNPy software, to express it in a disaggregated way. Such step will be discussed in next session, and it is the last part of the initial theoretical analysis of this thesis work.

3.3.3 Disaggregated model

As anticipated, the final outcome of this work is to add the model feature to the software of GNPy. To do that it is necessary to express the SNR of the total system in a disaggregated manner. This to allow the usage of a metric that can be accumulated step-by-step as the DT computes the propagation effect crossing the network elements. First of all it is useful to recall the definition of the disaggregated ISNR given in Equation 1.5.

$$ISNR = \sum_{i=1}^{M} ISNR_i \tag{3.76}$$

Which is the target of the current session, namely to derive a QoT metric based on the disaggrgated definition of ISNR. Taking as a reference the diagram in Figure 3.2, it has been shown in Equation 3.68 that on each i-th noise field contribution acts the Jones operator T_{ni}. Regarding the transmitted signal $\vec{s}$, in Equation 3.72 it has been shown that no Jones operator acts on it thanks to the DSP action that fully recovers it. As first step, the expression of ISNR is derived in terms of

electromagnetic fields using Jones formalism for both the polarization axes x and y.

$$\begin{aligned} ISNR_x &= \frac{1}{GSNR_x} \\ &= \frac{\sum_{i=1}^{M} |T_{n,i}\vec{n}_i \cdot \hat{x}|^2}{|\vec{s} \cdot \hat{x}|^2} \\ &= \frac{\sum_{i=1}^{M} |\left(T_{(1\to i-1)}\right)^{-1} \vec{n}_i \cdot \hat{x}|^2}{|\vec{s} \cdot \hat{x}|^2} \\ &= \sum_{i=1}^{M} \frac{\left|\left(T_{(1\to i-1)}\right)^{-1} \vec{n}_i \cdot \hat{x}\right|^2}{|\vec{s} \cdot \hat{x}|^2} \end{aligned} \tag{3.77}$$

The computation fot y-axis is symmetric, therefore the metrics to accumulate for both the polarizations are:

$$ISNR_{x,i} = \frac{\left|\left(T_{(1\to i-1)}\right)^{-1} \vec{n}_i \cdot \hat{x}\right|^2}{|\vec{s} \cdot \hat{x}|^2} \tag{3.78}$$

$$ISNR_{y,i} = \frac{\left|\left(T_{(1\to i-1)}\right)^{-1} \vec{n}_i \cdot \hat{y}\right|^2}{|\vec{s} \cdot \hat{y}|^2} \tag{3.79}$$

Working with fields and random vectors such as $\vec{n}_i$ is not simple, both for software implementation on GNPy and for Monte Carlo simulation purposes, as it will pointed out in chapter 5. Therefore, as anticipated in the introduction, working with powers and intensities is more effective. To conclude the derivation of the disaggregated model it is needed to pass from field to power formalism, using power transfer matrices. This can be done converting the terms on the ISNR accumulated metrics of Equation 3.78. The correctness of such process is proved by demonstrating the equality between the disaggregated GSNR with respect to the system SNRs computed in Equation 3.74 and Equation 3.75:

$$\begin{aligned} GSNR_x &= ISNR_x^{-1} = \left(\sum_{i=1}^{M} \frac{\left(T_{(1\to i-1)}^{-1}\right)^{\dagger} T_{(1\to i-1)}^{-1} \odot \vec{p}_{n,i} \cdot \hat{x}}{|\vec{s} \cdot \hat{x}|^2} \right)^{-1} \\ &= \frac{1}{2} \frac{1}{\sum_{i=1}^{M} \left(T_{(1\to i-1)}^{-1}\right)^{\dagger} T_{(1\to i-1)}^{-1} \odot \vec{p}_{n,i} \cdot \hat{x}} = SNR_{RX,x} \quad \square \end{aligned} \tag{3.80}$$

Consequently, regarding y-polarization:

$$GSNR_y = ISNR_y^{-1} = \left(\sum_{i=1}^{M} \frac{\left(T_{(1\to i-1)}^{-1}\right)^{\dagger} T_{(1\to i-1)}^{-1} \odot \vec{p}_{n,i} \cdot \hat{y}}{|\vec{s} \cdot \hat{y}|^2} \right)^{-1}$$
$$= \frac{1}{2} \frac{1}{\sum_{i=1}^{M} \left(T_{(1\to i-1)}^{-1}\right)^{\dagger} T_{(1\to i-1)}^{-1} \odot \vec{p}_{n,i} \cdot \hat{y}} = SNR_{RX,y} \quad \square \quad (3.81)$$

Ovserving the structure of Equation 3.80 and Equation 3.81, it is possible to notice that such expression of the problem is equivalent to the diagram in Figure 3.3, where the ISNR is computed for a sequence of receivers, provided by DSP, distributed along the link.

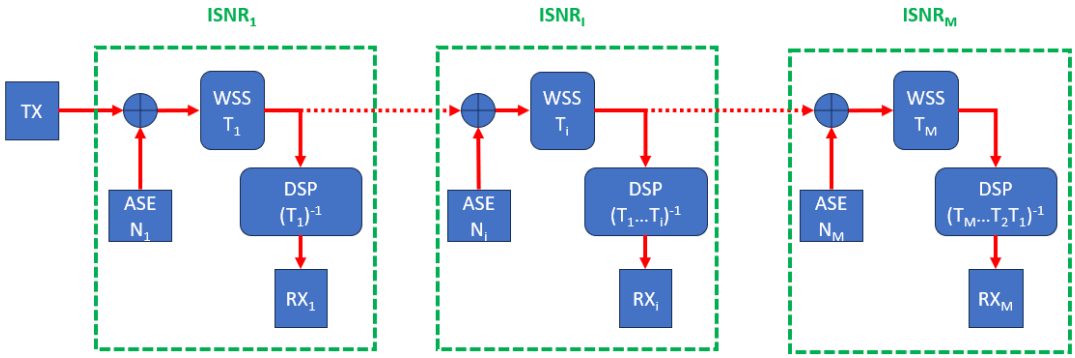

Figure 3.3: Disaggregated model block diagram

In conclusion, after the previous derivation, it can be asserted that a disaggregated model suitable to compute the GSNR of a sistem in which PDL and noise are inserted by WSSs along the path has been successfully developed. Such model, working with powers and intensities rather than Jones vectors for electromagnetic field, is suitable to build a software simulator to inspect the effect of PDL on a cascade of M PDL devices, through Monte Carlo analysis. Such work will be discussed in chapter 5, where the analysis results will be provided.

Chapter 4

Experimental Analysis

After deriving the mathematical tools for modelling PDL impairments in chapter 3, the work of this thesis focuses on an extensive experimental validation. A measurement campaign has been carried out at Links Foundation laboratories, within Politecnico di Torino. The scope of the campaign was to obtain a penalty in term of SNR for PDL, based on a setup composed by a cascade of WSS, investigating the effect of the noise introduction on the SNR distribution when the polarization alignment among the devices changes. For power budget reasons the maximum number of WSSs in the cascade has been set to three. Also the cases of a single WSS and two WSSs have been considered. All the measurements have been taken for four different frequencies of the input optical signal, and also the way in which the noise is injected in the setup has been changed, adding it at the transmitter stage, at the receiver stage and in a distributed way.

The work was divided into three stages, starting with a simple configuration and ending with the most complex one. The first one (setup number 0), described in section 4.2, with just a WSS and a polarization analyzer, was used to characterize the PDL behaviour vs frequency for each WSS. The second one (setup number 1), as it will depicted in section 4.3, aimed to characterize the PDL for the entire system vs frequency without the insertion of noise. In addition, setup number 1 has been used to set the measurements parameters such as the repetitions of measurements required by the system to obtain a stable measurement process. The final setup (setup number 2) was the most complex one. As it will be discussed in section 4.4, the insertion of noise, the usage of a transceiver, provided by DSP, has been the core of the measurement of PDL effect.

The measurement process has been carried out automatically exploiting the remote control of the instruments through a General Purpose Interface Bus (GPIB) [38]. All the scripts used to send commands to the instruments and to run the measurements procedures were coded in MATLAB. This approach allowed to automatize and parallelize the thesis work activities, saving time and

resources. Nevertheless, the measurement process took some weeks to be completed, due to its extension in terms of number of experiments and experiments complexity.

4.1 Devices

In this section the main devices adopted to perform the laboratory part of the thesis work is listed and some of their key features are underlined. All the devices are at Links Foundation optical laboratory, at OptCom research group disposal. Some devices, especially polarization scramblers, were required also by other research projects. Therefore, time management and laboratory sharing have been important to perform as much measurement as possible to give consistency to the laboratory validation.

4.1.1 WSS

The WSS adopted is the Cisco NCS 2000 16-port Flex Spectrum ROADM Line Card (NCS2K-16-WXC-FS), which is part of Cisco's Network Convergence System 2000 [39]. This line card supports advanced Reconfigurable Optical Add-Drop Multiplexer (ROADM) capabilities with features like colorless, contentionless, omnidirectional, and flexible spectrum (CCOFS) functionalities. These features enable software-driven wavelength routing, eliminating the need for manual interventions and allowing dynamic network adjustments. Its key features are:

- Colorless ROADM Ports: Ports are not frequency-specific, allowing for easier provisioning and dynamic restoration.
- Contentionless Add/Drop: Supports multiple wavelengths of the same frequency from a single add/drop device.
- Omnidirectional Ports: Wavelength rerouting can be managed entirely by software without physical fiber relocation.
- Flex Spectrum: Allows flexible spectrum allocation for single wavelengths or multicarrier superchannels, enabling more efficient use of available bandwidth.

A summary of the main specifications follows:

- Optical Specifications: Supports 96 channels spaced at 50 GHz with a total of 384 slices (4800 GHz). The card also offers various attenuation and power specifications.
- Physical Specifications: The line card occupies two slots, weighs 9.92 lb (4.5 kg), and has a maximum power consumption of 100W.

- Management: Features include LEDs for status indication and integration with Cisco Transport Controller for operations and maintenance.

4.1.2 Polarization scrambler and analyzer at TX side

To perform the PDL measurements of section 4.2 and section 4.3, a combination of a polarization analyzer and scrambler has been adopted at TX side. Namely, the chosen devices were the PM1000 Polarimeter [40] and the EPS1000 Polarization Scrambler/Transformer [41], by Novoptel. A brief list with their key features follows.

PM1000 Polarimeter:

- Measures all four Stokes parameters, with displays on the Poincaré sphere and in oscilloscope mode.
- Supports various modes for displaying Stokes vectors (normalized, exact, non-normalized).
- Features a 100 MHz polarization state sampling frequency and can record up to 64 million polarization states.
- Offers real-time display and various triggering options, suitable for automated long-term polarization transient assessments.
- Available as a standalone desktop unit, a module card, or an intellectual property (IP) core.
- Optional extensions include O-E-S-C-L-U band operation and tunable C&L band laser modules.

EPS1000 Polarization Scrambler/Transformer:

- Functions as a polarization scrambler with additional capabilities like polarization-dependent loss (PDL) measurement.
- Supports PDL measurement in different modes and is capable of high-speed polarization state changes.

Their combination is ideal for characterizing photonic integrated circuits (PICs) across multiple optical bands. The capability of synthesizing desired polarization states and conducting advanced polarimetry on devices under test is accompanied by the support of Mueller and Jones matrix measurements with high temporal resolution, as well as polarization mode dispersion analysis.

These devices are designed for precise polarization state measurements and manipulations in various optical testing scenarios, including those involving photonic

integrated circuits, optical ground wires, and complex polarization-dependent devices. They provide advanced features for long-term monitoring, real-time analysis, and automated testing, making them suitable for both laboratory and field applications.

4.1.3 Tunable laser

The transmitted signal in the first two setups illustrated in section 4.2 and section 4.3 is emitted thanks to a tunable laser of the Keysight 819xxA Series [42]. These lasers are designed for high-performance optical testing, particularly for characterizing optical devices at high power levels. They are capable of delivering high output power, with some models reaching up to +15 dBm, making them suitable for testing both active and passive optical components, including amplifiers and broadband devices. Each model covers various wavelength ranges across the S-, C-, and L-bands, with the 81960A model offering an extensive range from 1505 nm to 1630 nm.

One of the standout features of the 81960A model is its fast swept spectral loss measurement capability, which combines fast sweep speeds with dynamic accuracy. This makes it ideal for Dense Wavelength Division Multiplexing (DWDM) component measurements and real-time updates during testing procedures. The lasers in this series are known for their high dynamic accuracy, which is crucial for precise adjustments and calibrations of DWDM components. They support continuous sweep modes with wavelength logging, ensuring that measurements are both accurate and reliable.

The series also includes models with internal modulation features, which are particularly useful for time-domain extinction and transient testing of optical amplifiers. Features like coherence control help to avoid interference-induced power fluctuations, while Stimulated Brillouin Scattering (SBS) suppression allows for the launch of high-power signals into long fibers without causing impairment in time-domain measurements.

These lasers are designed with a modular approach, making them compatible with Keysight's mainframes, such as the 8163A/B and 8164A/B. This modularity provides flexibility and cost-effectiveness for both single-channel and DWDM applications. Additionally, the lasers feature built-in wavelength meters and dynamic power control loops, which enhance measurement precision and reproducibility.

4.1.4 Polarization scramblers within the optical link

The two polarization scramblers connected to the setup in section 4.3 and section 4.4 are responsible for changing the PDL alignment between the WXCs, so that it is possible to collect SNR distributions.

The first one is of the Thorlabs PL100 Series [43], a benchtop device designed for in-line deterministic polarization control. This instrument is crucial in applications where stable output polarization is required, regardless of variations in input polarization. It offers high precision, with a SOP accuracy of ±0.25° on the Poincaré sphere and a degree of polarization accuracy of ±0.25%. Additionally, it features low insertion loss of less than 1.1dB and a PDL of less than 0.05dB, ensuring minimal signal degradation.

The PL100 Series operates over a dynamic range from -20dBm to +15dBm and supports a wavelength range of 1200 to 1700 nm, making it versatile for different power levels and optical systems. It functions within an operating temperature range of 5 to 45°C, providing reliable performance across various conditions.

This device is particularly useful for deterministic polarization control and locking, serving as a modern replacement for traditional looped fiber (paddle) controllers. It is well-suited for applications such as SOP scrambling and coupling into polarization-maintaining fibers. The PL100S model uses a standard single-mode fiber output and can replace looped fiber controllers in various setups. For remote operation, the SOP Locker can be controlled via USB, with drivers available for multiple programming environments.

The second scrambler is one of the Agilent 11896A Polarization Controllers [44], which are essential tools for optical testing, particularly in applications requiring precise polarization adjustments. These controllers are designed to enhance the measurement accuracy of polarization-sensitive devices such as EDFAs, single-mode fibers, and modulators by allowing for automatic and manual adjustments of polarization states without altering optical power.

The Agilent 11896A operates within a wavelength range of 980 nm and 1250 to 1640 nm, offering a motorized polarization adjustment with minimal optical insertion loss. It is capable of fast measurements, rotating 360 degrees in less than half a second, making it suitable for applications like PDL measurements.

These controllers are equipped with user-friendly features such as manual adjustment capabilities, save/recall registers for quick state changes, and remote control options via GPIB. Their specifications highlight a commitment to precision, with characteristics like low insertion loss and high polarization extinction ratios, ensuring reliable performance across various optical testing scenarios.

4.1.5 Transceiver

To add the DSP functions to the final setup in section 4.4 and to inject the transmitted signal, measuring the BER, a state-of-the-art transceiver system has been chosen. This system is designed to handle the rapidly growing demand for video traffic and supports high-capacity, high-performance networking for various applications, including metro, long-haul, and submarine environments.

The transceiver supports up to 4.8 Tbps of client traffic and 4.8 Tbps of trunk traffic within a compact 2RU form factor, offering a significant increase in capacity over previous generations. In addition, the system allows fine control over modulation formats (from BPSK to 64-QAM) and baud rates (28Gbd/s to 72Gbd/s), enabling customized spectral efficiency and reach characteristics. The system supports a wide range of applications, from metro to long-haul and submarine, with software-configurable trunk line rates from 50G to 600G, while providing AES-256 encryption for secure data transmission, crucial for data privacy.

It offers comprehensive management tools, including streaming telemetry for real-time monitoring and headless operation to ensure uninterrupted data flow during software upgrades. The system is designed to operate within a wide range of environmental conditions and includes redundant power supplies and fans for high availability.

4.2 Setup 0: single WSS characterization

The first setup was built to characterize some Cisco WSSs in term of PDL vs frequency, in order to select the ones suitable for the PDL model validation. A frequency dependency of PDL has already been observed [26], thus this initial step has been necessary to characterize each WSS, also allowing a future software representation of them, which is discussed in chapter 5.

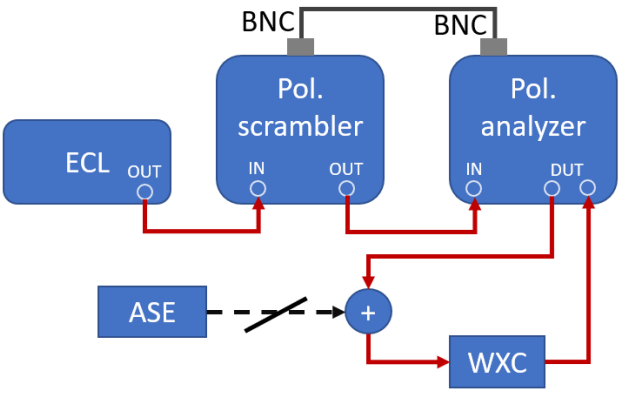

Figure 4.1: setup 0

Three Cisco WXC have been considered. Since each WXC can be used both in MUX and DEMUX mode, six possible PDL devices were available, namely:

- WXC number 2 MUX / DEMUX
- WXC number 3 MUX / DEMUX

- WXC number 4 MUX / DEMUX

Their specifics have already been discussed in section 4.1. The first experiment aimed to characterize their PDL vs frequency curve. In Figure 4.1 the setup is showed. A tunable laser was connected to the polarization scramble and analyzer, which were responsible to perform the PDL measurement. In Figure 4.1 it ca be seen that a coupler was inserted before the WXC under examination. This to characterize a setup as similar as possible to the ones that follow, since the final objective is to insert a certain amount of noise along the optical link. However, at this stage no ASE noise has been injected in the link, as it is pointed out by the black barred lines in Figure 4.1.

The measurement process is depicted in Algorithm 1. For each frequency the PDL measurement has been repeated 10 times, computing both the average and the standard deviation in order to produce errorbars when plotting the result. The frequency sweep ranges from 191.4 THz to 196 THz, considering 75 equispaced frequencies.

Algorithm 1 Characterization of PDL vs frequency for each Cisco WXC

```
1: for w in wavelength set do
2:     Laser wavelength ← w
3:     for i = 0; i < 9; i++ do
4:         PDL ← measure PDL
5:         Store measurement
6:     end for
7: end for
```

The measurement outcome is provided in Figure 4.2. It represents the PDL averaged each 10 measurements for all the frequencies considered in the sweep mentioned above. For each point, 90% confidence intervals have been plotted as errorbars. The first observation is that PDL introduced by each WXC is strongly frequency-dependent. The objective of this experiment is to select the WXCs and the frequencies of interest to proceed in the model experimental validation process. In order to ease the comparison with Monte Carlo simulations, there is the need to select some frequencies for which the value of PDL of each WXC is almost constant. This is the case for WXC 3 MUX, WXC 3 DEMUX and WXC 4 MUX in correspondance to approximatively 192 THz and and 195.5 THz. Therefore, these three WXC configuration have been chosen to carry out additional experiments. In addition, 191.5 THz and 194.5 THz were considered as frequencies too, since in these conditions, the chosen WXCs can be disposed to have an increasing and decreasing value of PDL along the devices cascade. The definitive WXC order has

been set to:

$$\text{WXC 3 DEMUX} \Rightarrow \text{WXC 3 MUX} \Rightarrow \text{WXC 4 MUX} \tag{4.1}$$

To summarize, the selected frequencies are:

$$191.5 \text{ THz}, \quad 192.0 \text{ THz}, \quad 194.5 \text{ THz}, \quad 195.5 \text{ THz}, \tag{4.2}$$

A final consideration is that the amount of PDL introduced by the considered WXCs is limited (around 0.2 dB), therefore if an EDFA is added to the setup to restore the signal power, its PDL has to be considered non-negligible and the amplifier must be characterized. This reasoning will come out later on, when dealing with the cascade of 3 WXC, which posed some challenges in term of power budget.

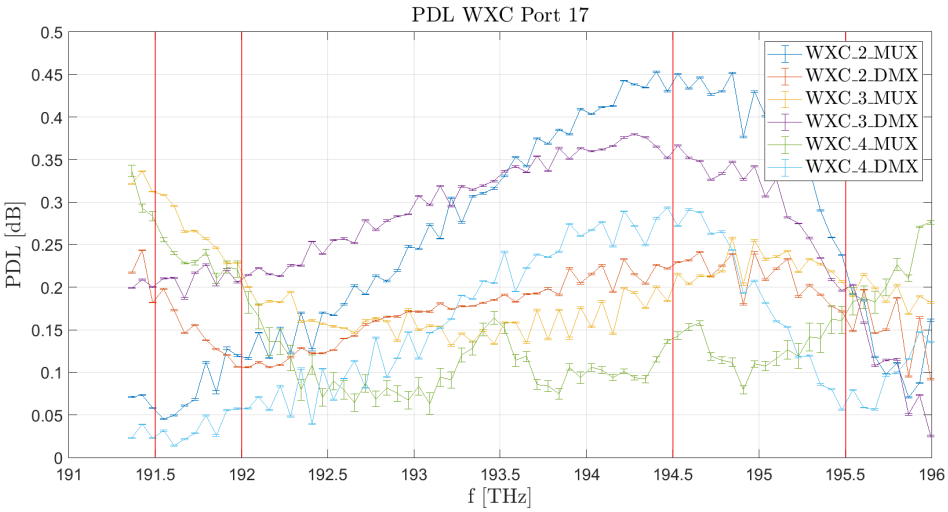

Figure 4.2: PDL vs frequency comparison among the available WXCs

The amount of PDL introduced by each WXC for each selected frequency, looking at Figure 4.2, is provided in Table 4.1. It is possible to notice, especially for 194.5 THz that the PDL is decreasing among the WXCs, and for the other frequencies it is almost stable.

4.3 Setup 1: cascade of WSS characterization

The second setup focuses on characterizing the cascade of WXCs, in term of the amount of PDL that is experienced by the laser signal without inserting any noise along the path. This part is important to set some key measurement parameters,

frequency [THz]	WXC 3 DMUX [dB]	WXC 3 MUX [dB]	WXC 4 MUX [dB]
191.5	0.20	0.31	0.28
192.0	0.21	0.23	0.22
194.5	0.37	0.22	0.14
195.5	0.20	0.19	0.18

Table 4.1: Amount of PDL for each of the selected WXCs for each frequency

such as the number of measurements to take in order to provide an accurate and reliable PDL measure. Not only, this part of the measurement process is also important to characterize the system in view of the comparison that will be carried out with the outcome of the Monte Carlo analysis. Indeed, the simulation has to be performed setting its system parameters to be as similar as possible to the laboratory system, to give a plausible comparison.

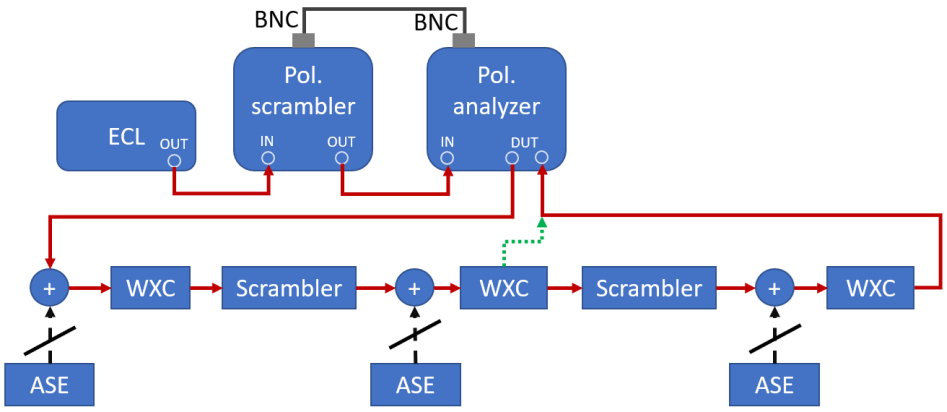

Figure 4.3: setup 1

The setup scheme is given in Figure 4.3. The transmitter part is the same as section 4.2, exploiting the tunable laser, the polarization scramble and the polarization analyzer. What changes is the number of WXCs inserted along the link. As in section 4.2, the optical splitters have been connected between the WXCs even if no noise is injected (signed with black barred lines), to characterize a system as similar as possible to the final setup. In addition, between the WXCs also two polarization scramblers have been connected. Such instruments have a pivotal role in the measurement process. As already anticipated, PDL is aligned with different angles in the WXCs, and this angle, in general, is not known and it is modeled as a uniform random variable. This misalignment of PDL is made random also by the optical fiber birefringence. The changes in PDL alignment along the path are time

varying, and depend also on external causes, such as vibrations. The scramblers within the link are responsible to recreate this environment in laboratory conditions, so that the signal generated by the laser crosses at each measure a different PDL alignment along the path. The scrambler at TX side instead plays a different role: it allows to change the polarization of the transmitted signal, exploring the Poincarè sphere, and measuring PDL through an opportune algorithm.

The green connection in Figure 4.3 represent the fact that both the cascade of two and three WXCs have been characterized. Two main test have been carried out:

- Keeping the scramblers fixed, repeat the PDL measure to select how many measurements are necessary to have a stable PDL mean and standard deviation.
- Activate the scramblers at each measurement in order to change the PDL alignment, then select the number of measurements for which the maximum and minimum of PDL are stable to be sure that the number of explored alignments is large enough.

The two experiments are summarized with the following algorithms:

Algorithm 2 Characterization of PDL's mean and standard deviation with fixed scramblers

```
for w in wavelength set do
    Laser wavelength ← w
    for i = 0; i < n_meas; i++ do
        PDL ← measure PDL
        Store measurement
    end for
end for
μ, σ ← compute mean and standard deviation from PDL measurements
```

The previous experiments have been repeated for different frequencies of the tunable laser, inclusing the four chosen in section 4.2, and for the cascade of two and three WXCs. The outcome of these tests follows.

4.3.1 Cascade of two WSSs

The first test aims to select the minimum number of measurements, with fixed scramblers, for which the PDL mean adn standard deviation are stable enough. In Figure 4.4 the mean for different frequencies and for an increasing number of measurements is reported. As it can be seen, such measurement is very stable, even

Algorithm 3 Characterization of PDL's minimum and maximum with polarization scrambling between measurements

for w in wavelength set **do**
    Laser wavelength ← w
    $PDL_{max} \leftarrow 0$
    $PDL_{min} \leftarrow \infty$
    for i = 0; i < n_{meas}; i++ **do**
        move polarization scramblers
        PDL ← measure PDL
        if $PDL > PDL_{max}$ **then**
            $PDL_{max} \leftarrow PDL$
        else $PDL < PDL_{min}$
            $PDL_{min} \leftarrow PDL$
        end if
    end for
    store PDL_{max} and PDL_{min} corresponding to the current frequency
end for

when few measurements are available. This holds for almost every tested frequency, except for 194 THz, which is not among the four frequencies chosen in Equation 4.2. The amount of PDL is not significant in this test, since scramblers were fixed. Therefore, a certain PDL alignment was kept fixed between the WXCs, among the all possible polarization alignments. The focus of the experiment was only on the measurement stability, which is satisfactory also when few measurements are taken. This is good in terms of required time to perform the measurement process, that can be saved limiting the repetition of the measure with fixed scramblers to less than 10 for the four selected frequencies in next steps.

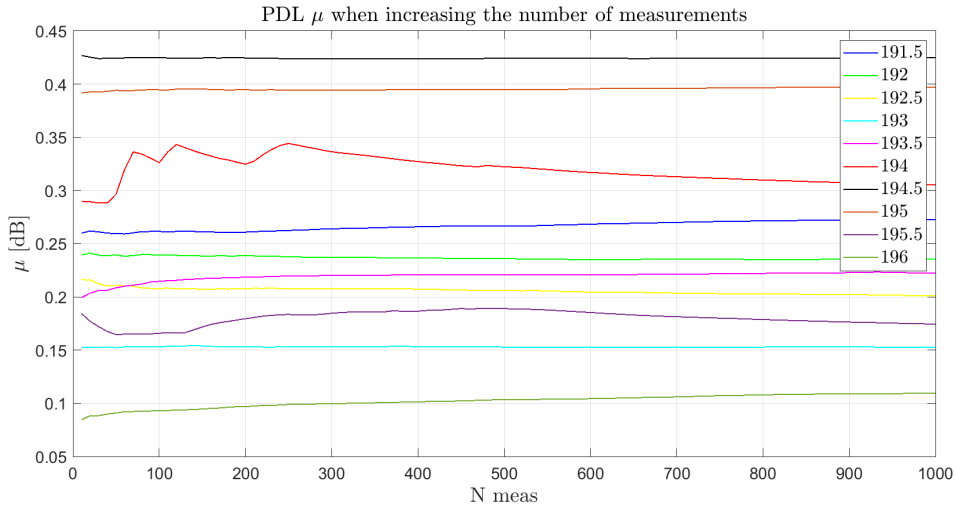

Figure 4.4: PDL mean with respect to the increasing number of measurements with fixed polarization scramblers

Regarding the standard deviation measurement, as it is depicted in Figure 4.5, its magnitude is reduced with respect to the PDL mean value. Comparing Figure 4.4 and Figure 4.5, chosing the most critical frequency, which is 194 THz, the PDL mean value stabilizes around 0.3 dB, while its standard deviation is always less than 0.07 dB and stabilizes around 0.045, therefore σ is 15% of μ. On the other hand, if the focus is on the four selected frequencies in Equation 4.2, this ratio is lower. For instance, considering 195.5 THz (the highest one), the ratio is equal to 11% while for 194.5 (the lower one) it is equal to 1.5%.

Not only, also in this case in which standard deviation is measured, less than 10 measurements are enough to find a sufficiently stable standard deviation value, therefore the time saving is confirmed also by this second test.

The last experiment carried out on this setup is meant to evaluate how many times it is needed to activate the polarization scramblers to explore as much as possible the Poincarè sphere, in order to collect significant distributions in the

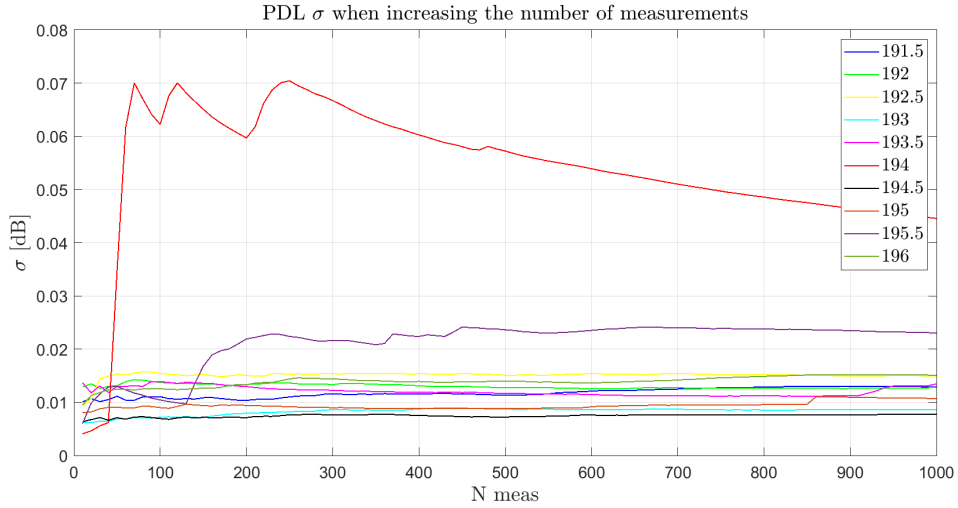

Figure 4.5: PDL standard deviation with respect to the increasing number of measurements with fixed polarization scramblers

next step discussed in section 4.4. This is obtained by measuring the maximum and minimum PDL value for increasing number of scramblers activations, whose result is reported in Figure 4.6. As it can be seen a large number of measurements is required, since even after 500 measurements the values of PDL maximum and minimum can increase significantly. Some frequencies are more stable than others: among the chosen ones, the most problematic are 194.5 THz and 195.5 THz, which show changes in, respectively, PDL min and max values after 500 measurements. On the other hand for 191.5 THz and 192 the situation seems to be more stable. Starting from these considerations, it has been decided to take at least 1000 measurements activating the scramblers when facing the situation in which 1 or 2 WXC are connected to the link. This condition was more than met in the successive experiments discussed in section 4.4, when more than 2000 measurements were taken to ensure an extensive exploration of the Poincarè sphere.

4.3.2 Cascade of three WSSs

Many of the considerations developed in subsection 4.3.1 hold also when three WXCs are inserted in the link. In Figure 4.7 and Figure 4.8 results for PDL mean and standard deviation versus number of measurements with fixed polarization scramblers are provided. In this case there is a slight difference in achieving stability, since more measurements are needed. Also the mean and standard deviation magnitudes are higher, which was expected since more elements are inserting PDL in the link. Nevertheless, the ratio between standard deviation and

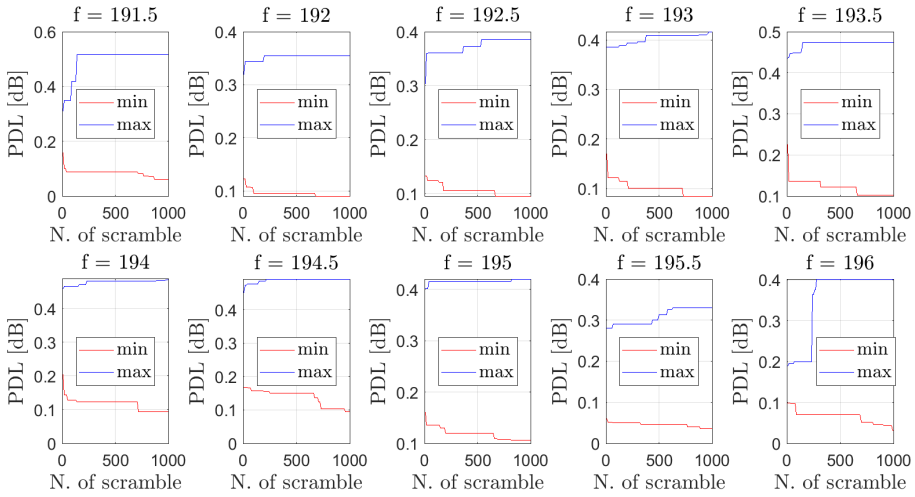

Figure 4.6: PDL max and min with respect to the number of times the polarization is scrambled

mean, which was mentioned in subsection 4.3.1, remains lower than 11% (which was the case when frequency was equal to 193.5), therefore the same considerations on time saving hold also in this case.

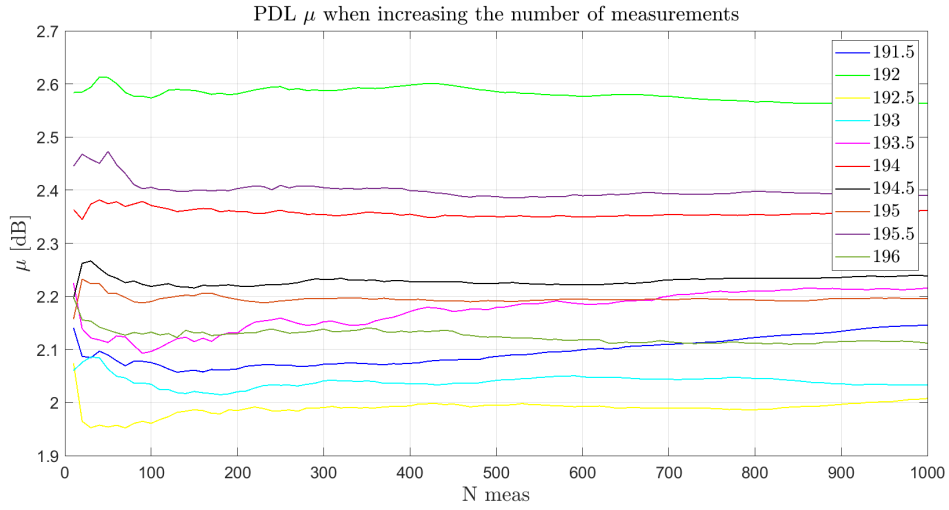

Figure 4.7: PDL mean with respect to the increasing number of measurements with fixed polarization scramblers

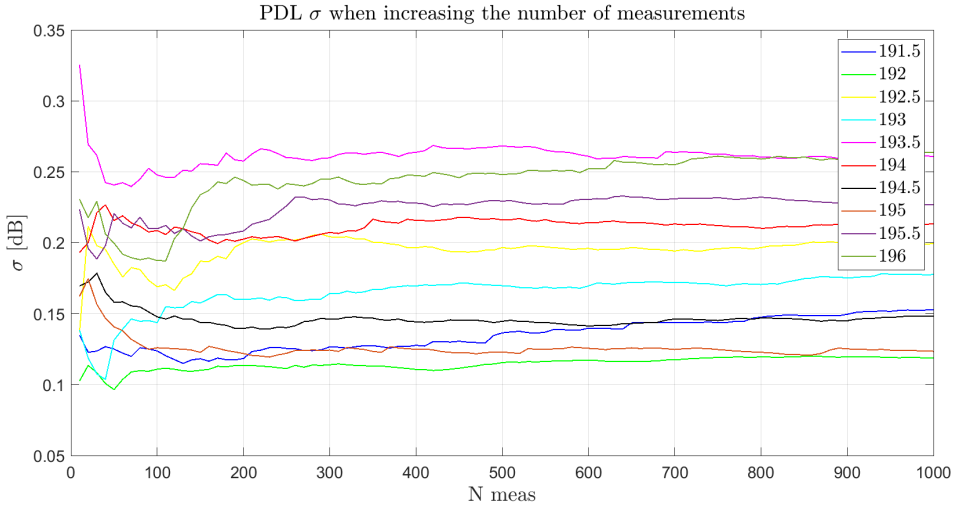

Figure 4.8: PDL standard deviation with respect to the increasing number of measurements with fixed polarization scramblers

Finally, Figure 4.9 depicts the last experiment carried on setup number 1. In this last case the outcome is, as expected, that with three WXCs an higher number of possible PDL alignment exists between the devices, therefore it is necessary to activate the polarization scramblers more time in order to explore the as much as possible the states of polarization. As in the case of two WXCs, 194.5 THz and 195.5 THz are the most critical frequencies among the four chosen ones, showing PDL maximum and minimum changes also very close to 2000 measurements. As a consequences, it has been established that at least 2000 measurements are needed when three WXCs are connected to the link, which was met in experiments described in section 4.4.

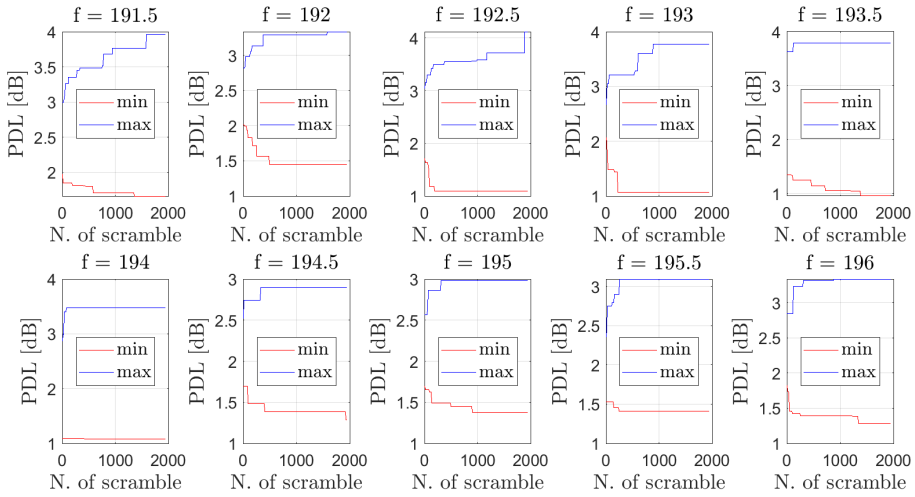

Figure 4.9: PDL max and min with respect to the number of times the polarization is scrambled

4.4 Setup 2: introduction of noise and DSP

The final set of experiments is the core of the laboratory validation of this thesis work. The aim is to study how the setup is affected by PDL impairment in term of OSNR, taking into account the effect of PDL on ASE noise when DSP is present to recover the transmitted signal at RX side.

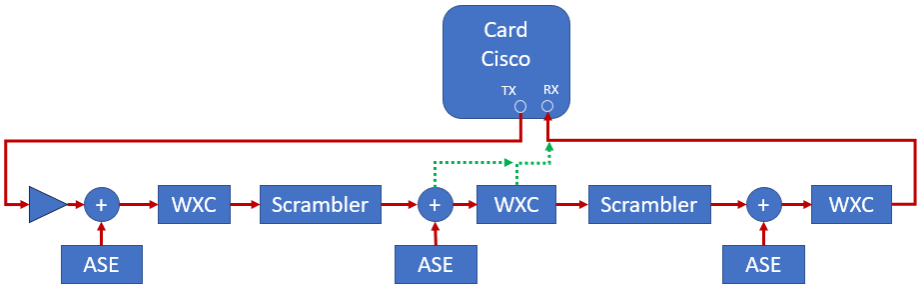

Figure 4.10: setup 2

The setup is showed in Figure 4.10, where it can be seen that the transceiver embedding DSP functions is a state-of-the-art linecard, which has been described in subsection 4.1.5. All the link is the same of what showed in Figure 4.3 for setup number 1. The only differences are the addition, at TX side, of an EDFA and the

connection of the ASE noise sources to the optical splitters, since in this final part noise has been injected within the optical link. The EDFA was necessary for power budget reasons: the linecard was not able to detect the signal since the RX power after the combination of WXCs, scramblers and splitters was under its sensitivity. The EDFA addition solved such problem, but it is necessary to consider that also the EDFA is both a noise source and a PDL device. For this reason it has been necessary to characterize the EDFA in terms of PDL and noise power. The EDFA operates in costant gain condition, with a gain equal to 17 dB. The EDFA output power during the measurement campain was equal to 12 dBm. To characterize the EDFA PDL, a total of 10 PDL measurements have been taken for each one of the four frequency of interest. Table 4.2 summarizes the characterization providing the average PDL for each frequency. Comparing the EDFA characterization with Table 4.1 it is clear that the amount of PDL introduced by the EDFA is not negligible with respect to the ones introduced by the WXCs. This will came out in the following sections, as the EDFA can be considered as an additional PDL element in cascade with the WXCs.

frequency [THz]	191.5	192.0	194.5	195.5
PDL [dB]	0.11	0.10	0.20	0.17

Table 4.2: Amount of PDL inserted by the upstream EDFA for each frequency

Looking at Figure 4.10, the green dashed lines point out that the experiment has been repeated for one WXC only, for two WXCs and for three WXCs, respectively connecting the linecard RX port to the first WXC, to the second and to the third ones. The experiment consisted on collecting the RX OSNR distributions, obtained through the linecard BER measurements, for all the four frequencies of interest reported in Equation 4.2. To do that, before each BER measurement both the polarization scramblers were activated in order to change the PDL alignement of the devices similarly of what has been done in section 4.3 to obtain the maximum and minimum value of PDL showed in Figure 4.6 and Figure 4.9. Each BER measurement has been repeated three times, keeping fixed the scramblers, averaging to obtain more reliability. The algorithm of the measurement process follows:

Regarding the noise injection, three strategies have been adopted, exploiting three VOAs connected to the ASE sources, namely:

- TX: all the noise injected before the WXCs.
- DISTR: noise distributed equally among the splitters.
- RX: all the noise injected in the last splitter, closer to the WXC at RX side.

Algorithm 4 BER measurements for OSNR distribution derivation:
N_{meas}: number of times the scramblers are activated
n_{meas}: number of measurements to be repeated while the scramblers are fixed

```
1: for w in wavelength set do
2:     Laser wavelength ← w
3:     for i = 0; i < N_meas; i++ do
4:         move polarization scramblers
5:         ▷ repeat with noise injection at TX, RX and distributed
6:         for mode in [TX, DISTR, RX] do
7:             BER ← 0
8:             for j = 0; j < n_meas; j++ do
9:                 BER ← BER_measured / n_meas
10:            end for
11:            store BER
12:        end for
13:    end for
14: end for
```

To ensure a correct noise injection, VOAs have been set in order to keep a fixed OSNR value in correspondence to the receiver, so that the received BER, measured by the linecard was around 10^{-4}. The OSNR values for each configuration are reported in Table 4.3. To obtain such effect, the signal and noise power have been measured at RX side for each frequency and noise injection strategy. Each noise source has been connected to a VOA to control the amount of noise power provided by each source. Then, the VOA attenuation values have been set in order to make the received OSNR matching the required one. In the case of distributed noise such process has been more complex, because the noise must be balanced among three different sources. When just one WXC, only the TX strategy has been adopted, since the only splitter included in the setup was the one right after the EDFA at TX side. When dealing with two WXCs, to follow the RX strategy all the noise was injected in the splitter preceding the second WXC, since the last one on the right side of Figure 4.10 was excluded from the link.

	1 WXC	2 WXC	3 WXC
TX	11.7 [dB]	11.7 [dB]	12.7 [dB]
DISTR	11.7 [dB]	11.7 [dB]	12.7 [dB]
RX	11.7 [dB]	11.7 [dB]	12.7 [dB]

Table 4.3: Received OSNR for each configuration and noise injection strategy

Some issues have been experienced during the measurement process. First of all, the transceiver could not operate 100% of the time, since sometimes it was necessary to reboot it for reasons that have not been determined. In addition, a significant amount of time was needed by the polarization scramblers: to change the polarization alignment a pause, ranging from 1 to 2 seconds, was waited. This, as anticipated in section 4.3, had been repeated more than 1000 times for each configuration (1, 2, or 3 WXCs) and for each frequency, in order to explore as much polarization alignment as possible. Such need led to measurement sessions that often lasted for many days. During this time, a linecard block could slow down even more the process. All the measurements have been collected in automated way, exploiting the remote connection of the setup devices, illustrated in section 4.1. Sections from 4.4.2 to 4.4.4 provide the OSNR distributions derived from the BER measurements obtained through the algorithm 4.

4.4.1 Back-to-back characterization and transceiver penalty

In this section, the process to obtain the OSNR distribution starting from the BER measurements collected by the transceiver is illustrated. There are two main reasons to perform the following analysis, instead of simply considering the OSNR and SNR measurements directly provided by the linecard:

- The card is way more accurate when measuring the BER rather than the OSNR.
- Through a back-to-back characterization, it is possible estimating the transceiver penalty, getting rid of it and then obtaining the OSNR distributions.

In order to get rid of the transceiver penalty, the same procedure described in [45] has been adopted. The first step is to collect all the back-to-back BER curves for all the frequencies of interests and for both the x and y polarizations. Then fitting the curves obtained from the measurements through the theoretical formula for the BER curve of DP-QPSK modulation, it is possible to estimate the transceiver penalty for each frequency. Such penalty, called intrinsic transceiver SNR (SNR_{TRX}) is computed as follows:

$$SNR_{TRX} = \left[\Psi^{-1}(BER) - SNR^{-1}\right]^{-1} \tag{4.3}$$

where BER and SNR are the back-to-back measurements, while Ψ is the theoretical BER formula for DP-QPSK, namely [46]:

$$\Psi(x) = \frac{1}{2} erfc\left(\sqrt{\frac{1}{2}x}\right) \tag{4.4}$$

The BER variations for the different frequencies and polarizations are depicted in Figure 4.11, with the fitting curved obtained to compute SNR_{TRX}. The complete set of estimated SNR_{TRX} is provided in Figure 4.12, wit the best-fit estimate of SNR_{TRX} at 17.05 dB. The variations observed in SNR_{TRX} across different frequencies are assumed to result from fluctuations introduced during measurement, while the differences between polarization states are attributed to polarization-dependent loss inherent in the B2B setup.

After determining the transceiver intrinsic SNR, it is possible to compute the value of OSNR from the BER measurements of the linecard, according to the following expression:

$$OSNR = \frac{1}{\frac{1}{2 \cdot erfcinv^2(2 \cdot 10^{BER})} - \frac{1}{SNR_{TRX}}} \tag{4.5}$$

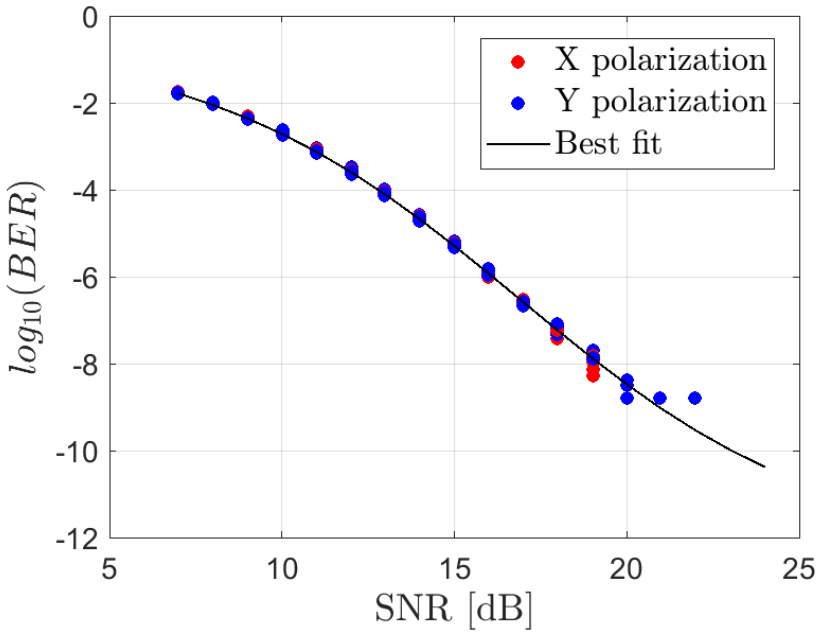

Figure 4.11: Back-to-back measurements over variable transmission frequency

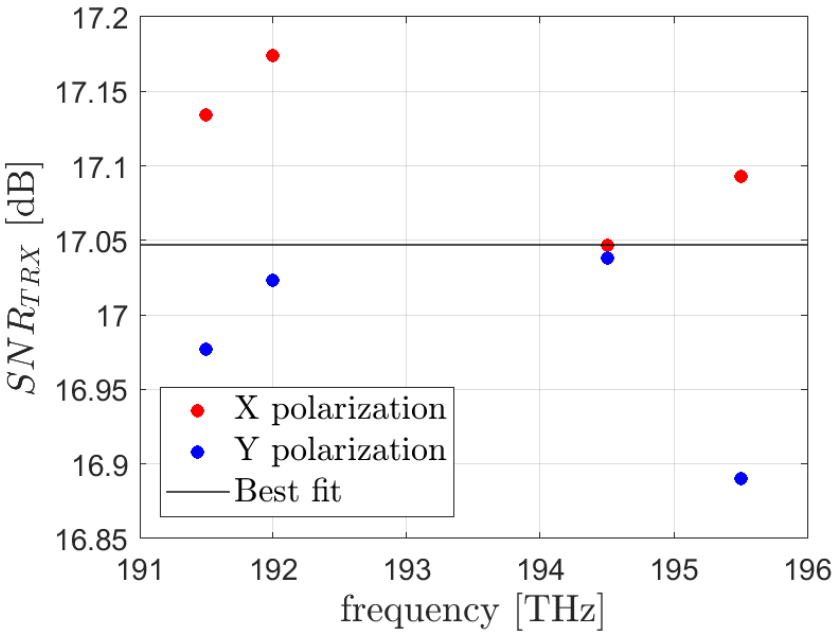

Figure 4.12: SNR_{TRX} estimation over variable transmission frequencies

In addition to the previous steps, the OSNR distributions have been processed by subtracting the moving average with a window of 10 OSNR values. This operation was necessary since the measurement campaign have been carried out in multiple days, therefore some fluctuations of BER mean value have been observed. After removing the moving mean, also some remaining outliers have been neglected. Such values were largely out of range and they were experienced in correspondence to the linecard switching on, thus, they are not significant at all. The OSNR distributions are provided in sections from 4.4.2 to 4.4.4, with some consideration on their shapes, related to the particular experimental conditions and the expected outcome.

4.4.2 Single WXC

In this section and the two that follow, the OSNR distribution obtained by the second setup showed in Figure 4.10 are provided. In Figure from 4.13 to 4.16, the case in which a single WXC introduces PDL is depicted. In this case a total amount of 1000 measurements have been taken, according to the observation of the measurement number made in section 4.3.

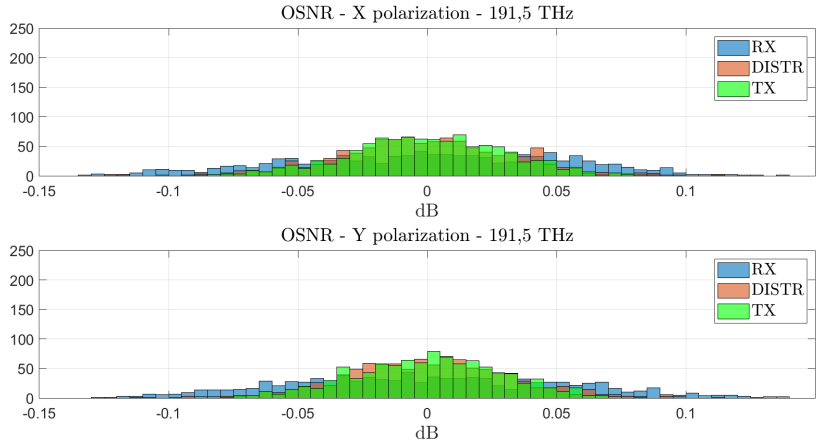

Figure 4.13: SNR distributions for 1 WXC and $f = 191.5$ THz

Many observations can be done. First of all, looking at the case in which all the noise is injected in the first splitter before the WXC, represented by the green color, it is clear that the distributions are stretched rather than beeing almost similar to a delta. According to what expected, the noise injected at TX side should experience the same amount of PDL of the transmitted signal, therefore the DSP is able to recover it, leading to a delta-shaped distribution of OSNR. This does not happen because of the EDFA upstream of the noise injection: as already seen in its characterization in Table 4.2, the amount of PDL, that it introduces in the link,

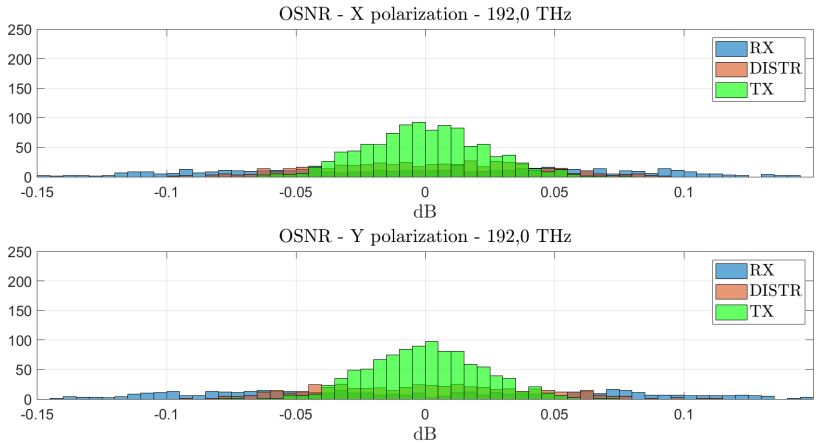

Figure 4.14: SNR distributions for 1 WXC and $f = 192.0$ THz

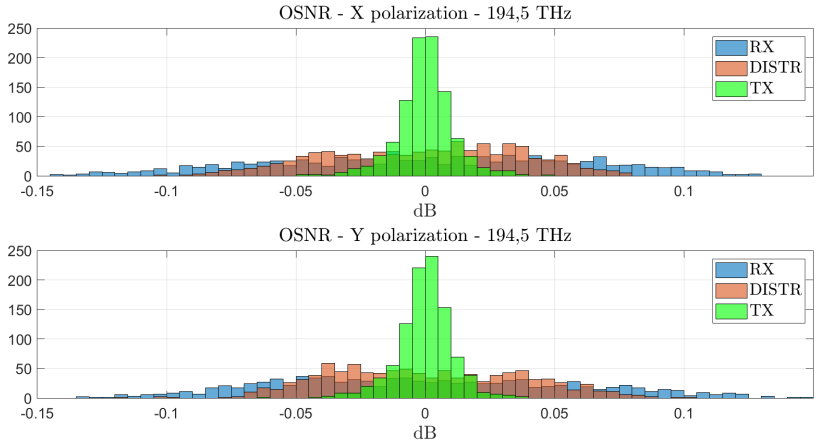

Figure 4.15: SNR distributions for 1 WXC and $f = 194.5$ THz

is not negligible with respect to the one introduced by the WXCs. This leads to the fact that the considered setup can be considered as id two PDL devices are posed in cascade, rather than a single one. In additon, it can be observed that the distributions shape is variable with the frequency. This is as expected, since PDL is frequency and port dependent, as seen in section 4.2. The fact that at lower frequency (191.5 THz and 192.0 THz) distributions are more stretched than the cases with higher frequencies (194.5 THz and 195.5 THz) is not trivial, and does not depend only on the EDFA PDL introduced at that frequencies. The effect is a consequence in how the PDL of the EDFA interacts with the PDL introduced by the ASE sources. This kind of analysis is out of the scope of this master thesis

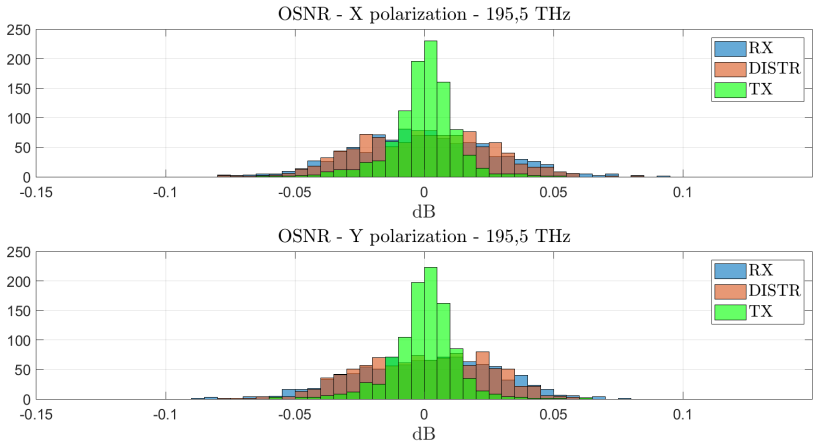

Figure 4.16: SNR distributions for 1 WXC and $f = 195.5$ THz

work, therefore it is left for further investigations.

The last observation regards the relative position of noise and PDL injection. Comparing the three strategies (namely TX, RX and DISTR), the case in which the OSNR is more spread over the mean value is when the noise is closer to the receiver, thus when considering RX strategy. This means that, looking at the negative part of x-axis, when noise is added after the PDL devices (or, likewise, when PDL is added before) in a larger number of cases the expected OSNR could be way lower than the reference one, which is represented by the mean value of the distribution. This is pivotal when determining a system margin based on PDL impairment, which is the next step to carry out after the current thesis work. Regarding the DISTR strategy, which represents the most common case when amplifiers introduce noise between network nodes in which WSSs are placed, it can be observed that the distribution is bell-shaped, which is interesting to compare with the mathematical model outcome that will be showed in chapter 5. To anticipate such results, the bell shape is in accordance to the mathematical model developed, validating the theoretical analysis of chapter 3.

4.4.3 Cascade of two WXCs

In this section the case in which two WXC inject PDL in the link is considered. As already stated in subsection 4.4.2, the presence of the EDFA upstream, which is represented in Figure 4.10, leads to the fact that this case is equivalent to when three PDL elements are present in cascade. Figures from 4.17 to 4.20 depicts the OSNR distributions, obtained through the processing described in subsection 4.4.1. In this case the number of measurements was equal to 2000 a part of the case of

194.5 THz, for which 1600 measurements have been taken.

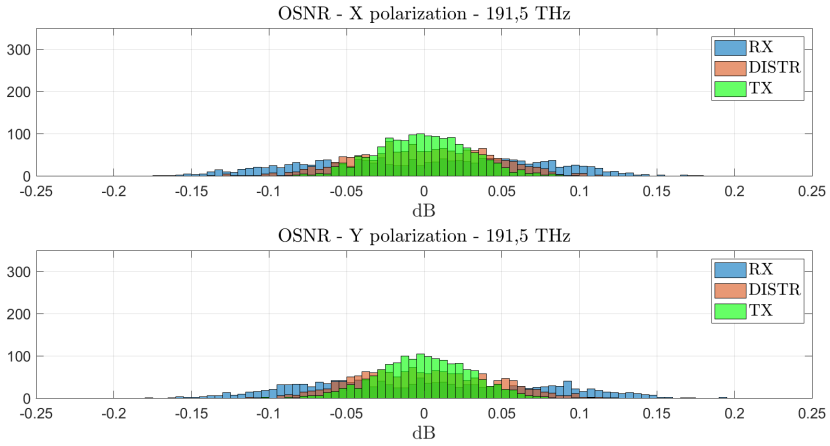

Figure 4.17: SNR distributions for 2 WXC and $f = 191.5$ THz

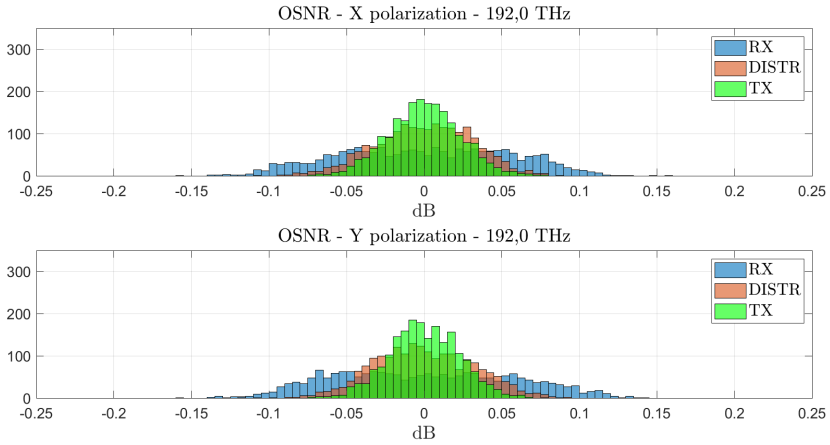

Figure 4.18: SNR distributions for 2 WXC and $f = 192.0$ THz

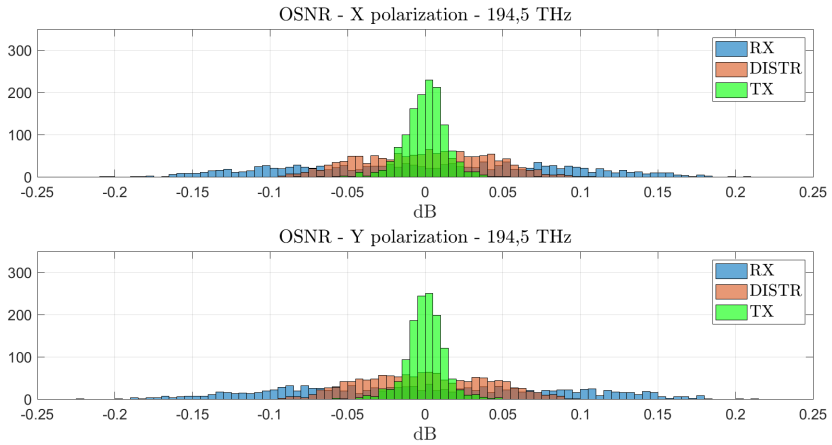

Figure 4.19: SNR distributions for 2 WXC and $f = 194.5$ THz

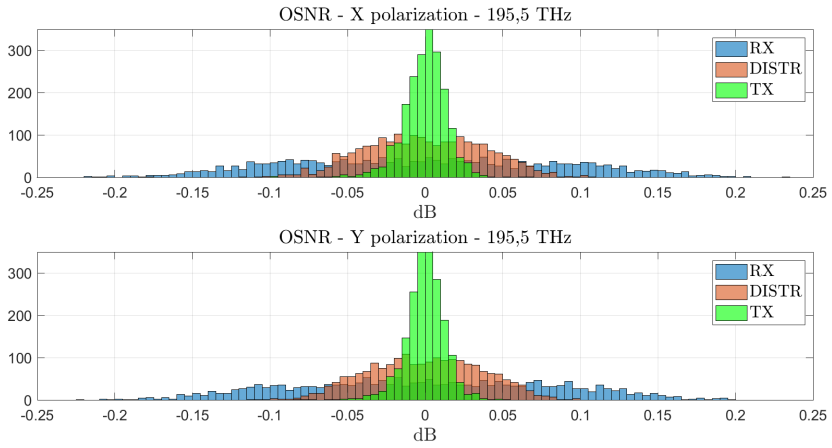

Figure 4.20: SNR distributions for 2 WXC and $f = 195.5$ THz

The comments provided in subsection 4.4.2 are still valid in this second case. Both the stretch for TX noise injection strategy and for the frequancy change are observed in the same way in this experiment. An additional comment is that, looking at the distribution extension, this second case with two WXCs is larger than the one with a single WXC. This is as expected, since the PDL effect of the WXCs superposes, even if it does not sum up.

4.4.4 Cascade of three WXCs

In this section three WXCs have been posed in cascade, according to the setup in Figure 4.10. This last measurement campaign has been the most extended one, due to the fact that the larger is the number of PDL elements, the higher is the number of possible alignment of PDL alignments among the devices. As pointed out in section 4.3, for this last case it has been found that more than 1000 measurements are required. Therefore, a total of 2600 measurements has been taken, in order to ensure an exploration of the PDL alignments as complete as possible. Figures from 4.21 to 4.24 provide the OSNR distributions. Also in this case the procedure followed to obtain them has been the one illustrated in subsection 4.4.1. Again, in this last case the observations are similar to the ones provided in subsection 4.4.2 and subsection 4.4.3, confirming the correctness of such conclusions.

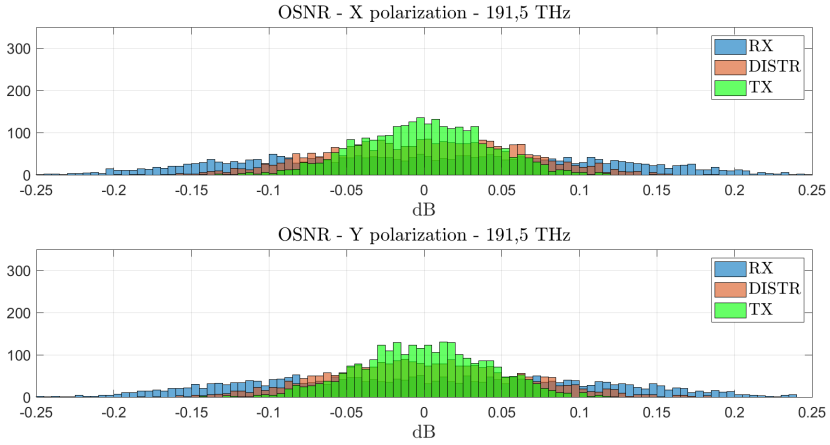

Figure 4.21: SNR distributions for 3 WXC and $f = 191.5$ THz

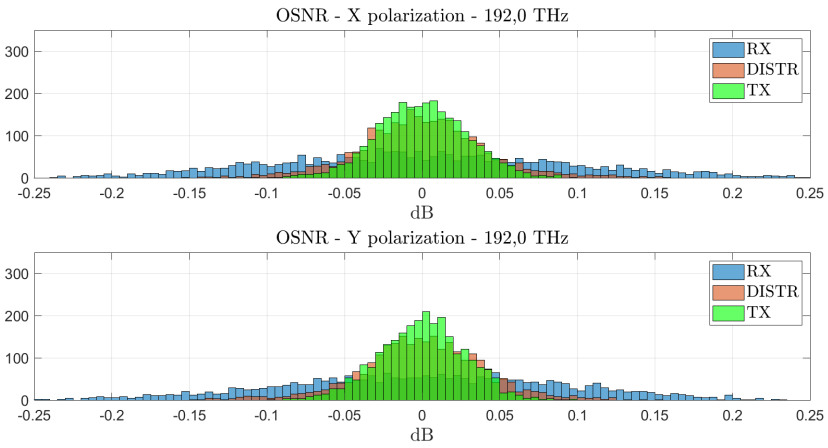

Figure 4.22: SNR distributions for 3 WXC and $f = 192.0$ THz

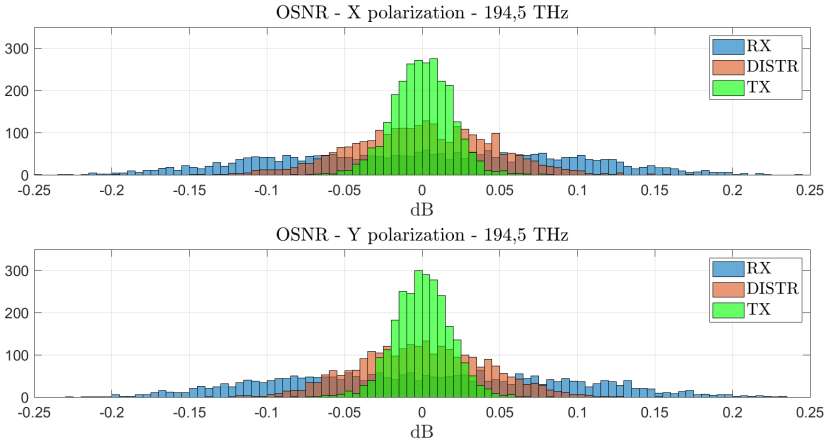

Figure 4.23: SNR distributions for 3 WXC and $f = 194.5$ THz

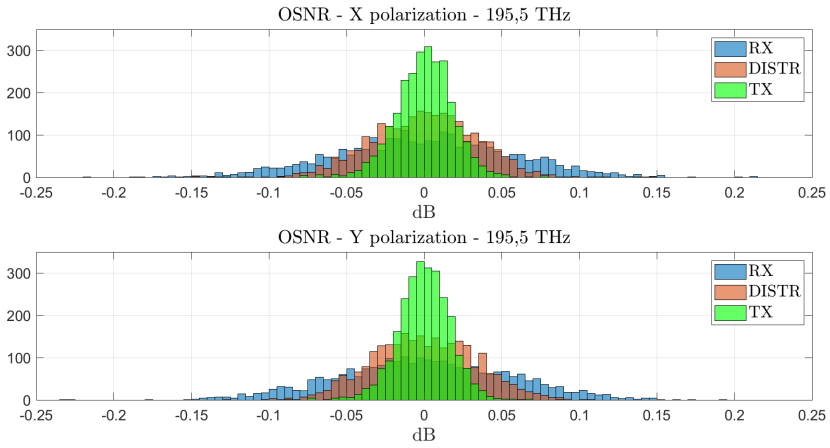

Figure 4.24: SNR distributions for 3 WXC and $f = 195.5$ THz

Chapter 5

Monte Carlo Analysis

As a final step of this thesis work, a software simulator of a cascade of WSSs has been developed. Such simulator, based on the mathematical model developed in chapter 3, aims to study the effect of PDL in conditions that cannot be investigated in laboratory due to the large number of considered elements in cascade. Such target is achieved through the possibility to perform a Monte Carlo analysis, based on the statistical characterization of the PDL phenomena. In addition, this first step allows a comparison between the outcome of the theoretical and the experimental analysis previously carried out. Such last work is also a required milestone in order to include the PDL effect in GNPy DT transmission model. The focus of the Monte Carlo campaign has been the case in which PDL and noise are inserted within the optical link in a distributed way, therefore each WSS, representing a network node, is followed by a noise source, representing the amount of ASE noise due to the EDFAs amplification.

The Monte Carlo campaign has been divided into three steps. First of all, the amount of inserted PDL is uniform among the WSS, fixed to a certain value. This choice, that simulates an environment similar to the laboratory phase, embed the stochastic nature of PDL in the PDL alignment among the different WSSs. Successively, another grade of complexity is added, in order to go beyond the laboratory analysis, adding a stochastic effect to the PDL value itself, which is modeled as a maxwellian random variable with certain mean and standard deviation based on the measurements previously performed [26]. Lastly, following the intuition developed in chapter 4, in which it came out that PDL penalty depends on the reciprocal insertion of noise and PDL, some trials have been performed analyzing the OSNR distributions when PDL inserted by WSSs is increasing or decreasing along the link.

The simulator structure is very simple and it is represented in Figure 5.1. A span, in this case, is defined when considering a couple composed by a WSS block and a noise block, as it is pointed out in the block diagram. Each WSS block

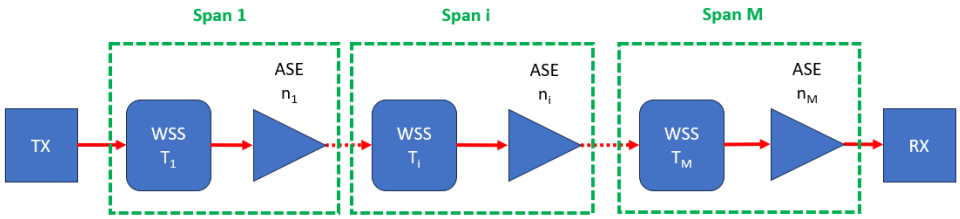

Figure 5.1: Monte Carlo simulator block diagram

is responsible to create a PDL Jones matrix, according to Equation 3.36 and Equation 3.38, which are reported here for clarity.

$$l_{x,i} = l_M = L * \frac{2 * pdl_i}{pdl_i + 1} \tag{5.1}$$

$$l_{y,i} = l_m = L * \frac{2}{pdl_i + 1} \tag{5.2}$$

$$T_i = \begin{bmatrix} \cos\theta_i & \sin\theta_i \\ -\sin\theta_i & \cos\theta_i \end{bmatrix} \begin{bmatrix} \sqrt{l_{x,i}} & 0 \\ 0 & \sqrt{l_{y,i}} \end{bmatrix} \begin{bmatrix} \cos\theta_i & -\sin\theta_i \\ \sin\theta_i & \cos\theta_i \end{bmatrix} \tag{5.3}$$

Both when PDL insertion is uniform or when it is stochastic, the angle θ, which represents the PDL alignment for a certain WSS, is always uniform distributed and extracted at each Monte Carlo run:

$$\theta_i \sim \mathcal{U}([0, 2\pi]) \tag{5.4}$$

Regarding the value of PDL, when **uniform insertion** is considered, it is fixed to a value equal to **0.2 dB** for all the WSSs. On the other hand, when a stochastic characterization of PDL is added to the Monte Carlo analysis, the PDL value is maxwellian-distributed as depicted in Equation 5.5, where the values of σ is taken from a previous characterization of WSSs PDL [26].

$$pdl_i \sim \mathcal{M}(\sigma) \quad \sigma = 0.14 \text{ dB} \tag{5.5}$$

For each run for each WSS a value of θ_i and of pdl_i are extracted randomly. Then the final OSNR is computed for an increasing number of spans and the process is repeated thousands of times, in order to derive OSNR distribution, simulating what happened in the laboratory analysis of chapter 4. The case of uniform PDL requires quite less runs compared to when PDL is stochastic, because of the lower number of possible cases, having just a single aleatory quantity.

The noise blocks, represented by the triangles in Figure 5.1, are responsible for the noise injection and for the output noise power computation. The output power of each noise contribution is computed through the formula derived in Equation 3.64, which is also reported here for clarity:

$$\vec{p}_{out,x,i} = \left(T^{-1}_{(1\to i-1)}\right)^{\dagger} T^{-1}_{(1\to i-1)} \odot \vec{p}_{n,i} \cdot \hat{x} \tag{5.6}$$

$$\vec{p}_{out,y,i} = \left(T^{-1}_{(1\to i-1)}\right)^{\dagger} T^{-1}_{(1\to i-1)} \odot \vec{p}_{n,i} \cdot \hat{y} \tag{5.7}$$

Then the noise contributions are summed up through the propagation simulation, according to the disaggregated model of Equation 3.71:

$$\vec{p}_{n,TOT} = \sum_{i=1}^{M} \left(T^{-1}_{(1\to i-1)}\right)^{\dagger} T^{-1}_{(1\to i-1)} \odot \vec{p}_{n,i} \tag{5.8}$$

Finally, the GSNR is computed, keeping the transmitted signal power unchanged, since DSP is assumed to be at the end of the link, recovering the information signal power. The process is repeated for each run. In term of computational time the simulator is pretty fast, since simple matrix multiplications are performed. For this reason the developed model is not only effective in describing PDL, but also efficient, leading itself to be used also in real-time applications for GNPy.

5.1 Uniform PDL insertion

The first step is the case in which each WSS introduces the same mount of PDL. To simulate a realistic environment, the value of PDL for each block has been set to **0.2 dB**, similarly to what obtained in characterizing the real Cisco WXCs in section 4.2. The signal power has been set to **12 dBm**, also recreating a laboratory-like simulation, while each noise contribution has been set to **-30 dBm**, which is also a reasonable quantity in term of realness. The output GSNR distributions have been computed for a number of span that ranges from 1 to 12, and a total of 25000 runs have been performed. In Figure 5.2 and Figure 5.3 the OSNR distributions are provided. The first observation, looking at the case of just one span is considered, is that the distribution shape appears to concentrate far away from its mean value. This behaviour, as the number of WSSs increases, leaves place to a bell-shaped distribution, which becomes wider with the number of WSSs. Such growth is not linear, and tends to saturate, which is reasonable, since the randomness of PDL alignment causes compensations and deletions in term of PDL effect. The higher is the number of PDL terms, the more unlikely are the worst and best cases in which PDL is completely aligned and sums up or when it is oppositely aligned and cancels out. Therefore the bell width increment starts to drop when considering a large number of spans. This case is interesting to analyze mainly to compare

the results with the outcome of the experimental analysis of chapter 4, and to understand how the PDL alignment acts in the process, since the only aleatory quantity is the angle θ, which models the position of PDL with respect to the two main polarization axes.

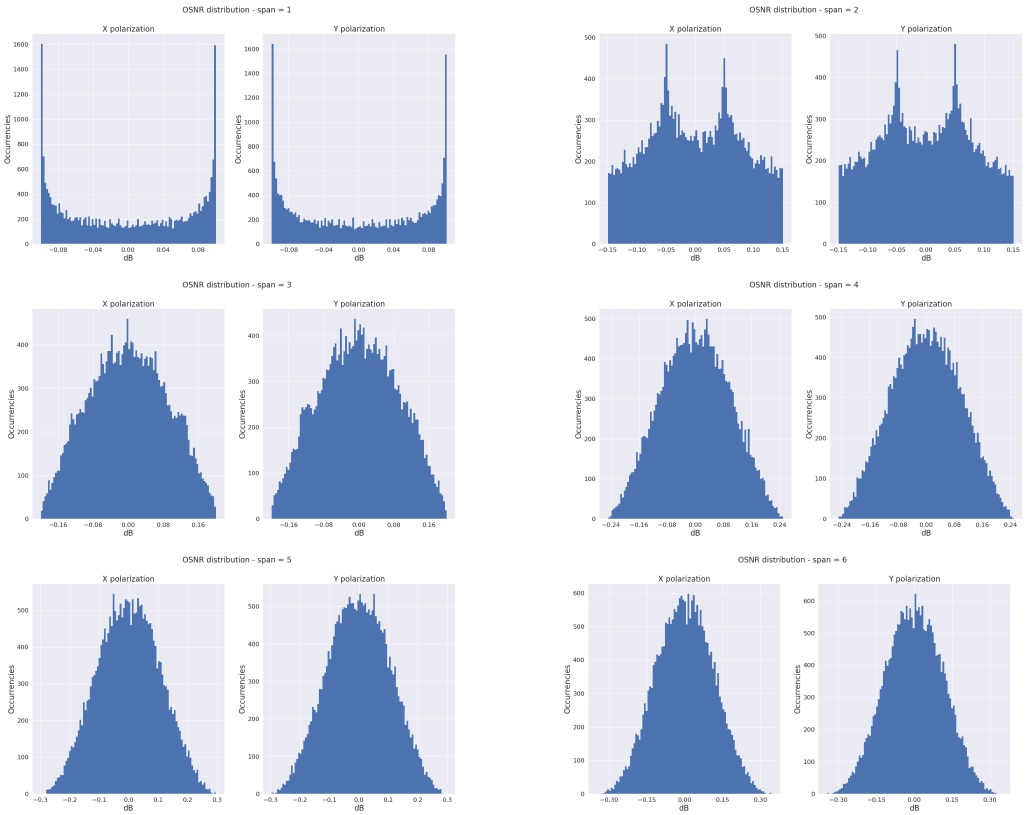

Figure 5.2: Monte Carlo run results for uniform PDL from 1 span to 6

The uniform PDL case is helpful also to test the correctness of the mathematical model, comparing it with the laboratory analysis outcome. When considering the cascade of three WXCs plus the EDFA studied in Figure 4.10, the distribution width in Figure 4.21, 4.22, 4.23 and 4.24 is around 0.15 dB. Such value is comparable with the case in which the simulator computes the OSNR distribution for three spans in Figure 5.2, where its width is around 0.16 dB, with the same launching power, similar values of inserted PDL and similar values of noise power. The laboratory case presents some differences, due to the realistic environment, but the bell shape and its width provided by the model are in accordance with the experiment. Still, such case is not the most realistic one. Since PDL is frequency, port and device dependent, the general case is when its value is also a stochastic quantity, modeled as a random variable, which is treated in the following discussion.

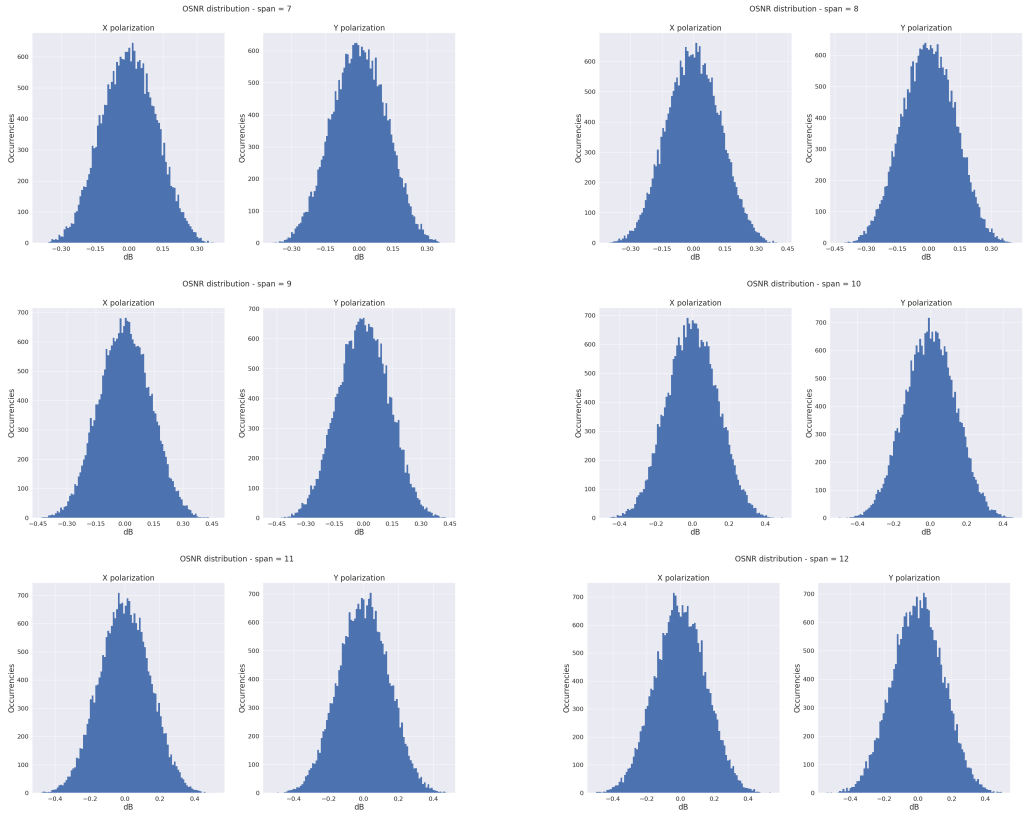

Figure 5.3: Monte Carlo run results for uniform PDL from 7 span to 12

5.2 Stochastic PDL insertion

As anticipated, the most realistic scenario is when PDL inserted by each WSS is modeled as a random variable. In particular, according to the characterization in [26], a reasonable model for PDL probability distribution is a Maxwellian-shaped PDF with standard deviation equal to **0.14 dB**, as showed in Equation 5.5. All the remaining parameters, such as signal power and noise power are kept the same as section 5.1, so that it is possible to distinguish the additional effect of PDL randomness, in addition to its random alignment. The number of runs has been increased, because of the presence of two stochastic quantities, to 50000 runs.

All the OSNR distributions are provided in Figure 5.4 and Figure 5.5. It can be noticed that the bell shape can be observed also in this case, even considering the case of just one and two spans. This facts suggests to hypothesize a kind of gaussianity in the distributions, when stochastic behaviour is embedded in PDL. This allows to consider a formulation of PDL penalty easier to compute. The exact expression of such penalty is beyond the scope of this thesis work, and will

be treated in further works and publications. Therefore, as last comment, it can be observed that the distributions, either in this case and in section 5.1 are not sufficiently smooth, which leads to the conclusion that the number of runs must be incremented for a better analysis.

This treatment of PDL as a random variable underlines the power and the importance of the Monte Carlo paradigm. It would be impossible to carry such analysis experimentally, because of the practical difficulties in terms of available devices and time to collect all the necessary measurements. The developed model allows to predict and study a phenomena through the simulator, which simplifies the understanding of PDL problem.

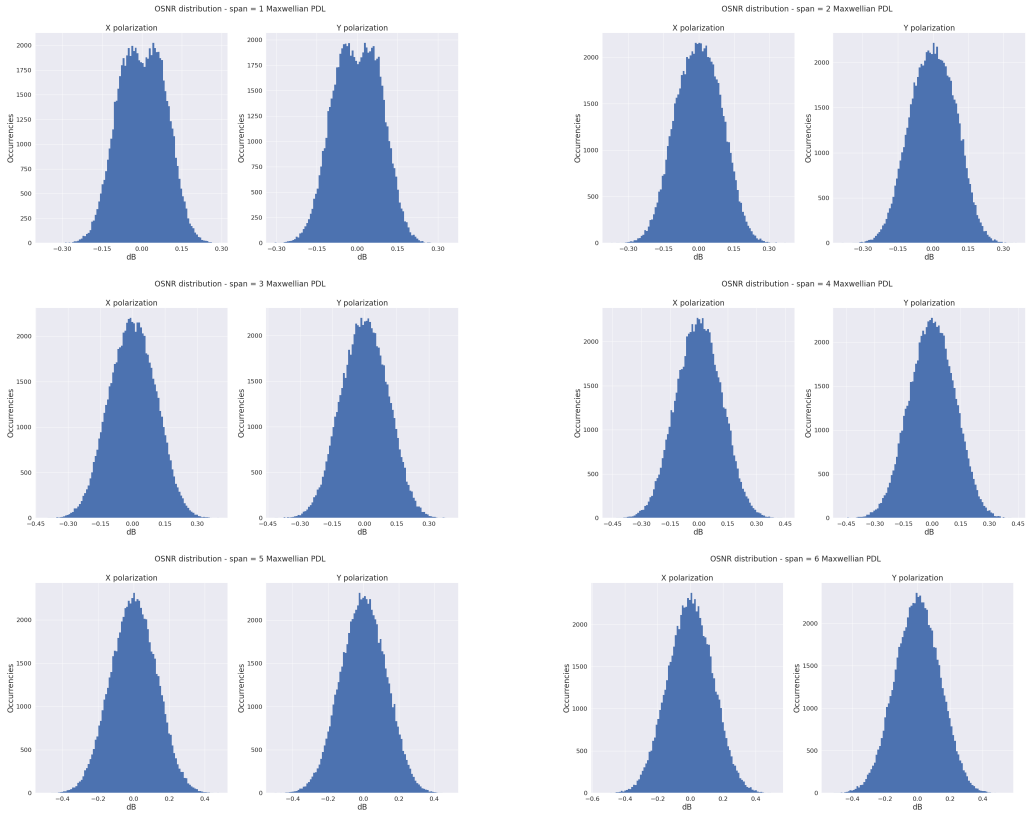

Figure 5.4: Monte Carlo run results for Maxwellian PDL from 1 span to 6

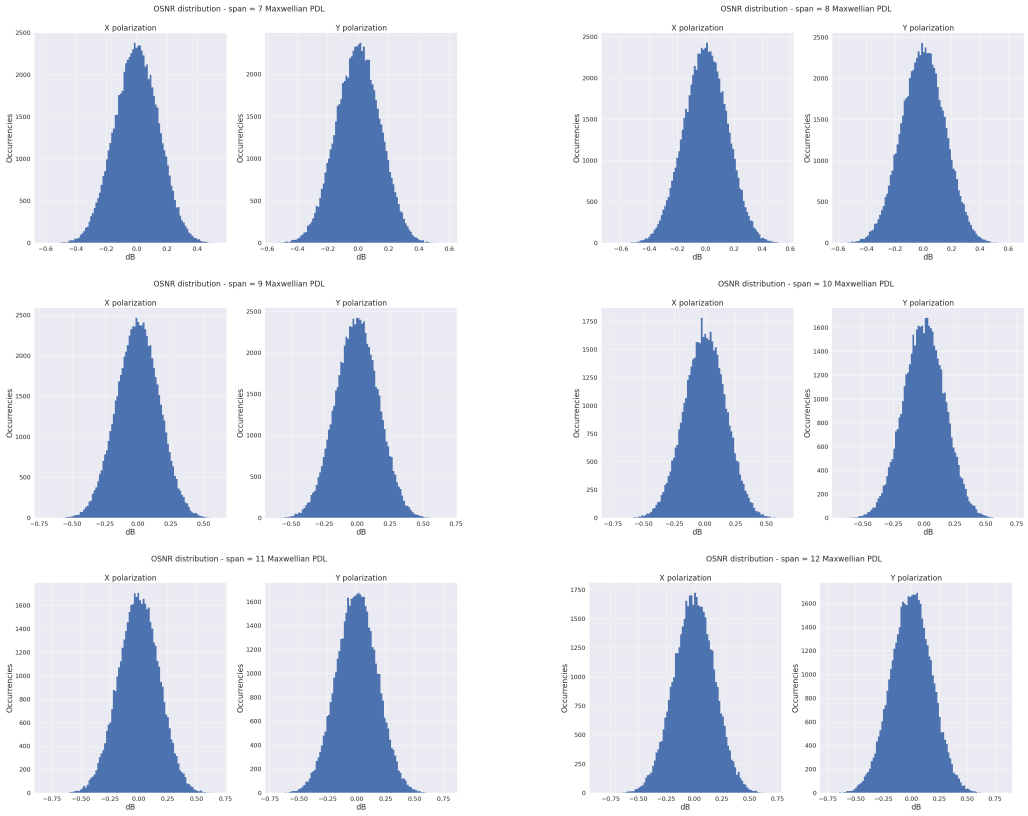

Figure 5.5: Monte Carlo run results for Maxwellian PDL from 7 span to 12

5.3 Increasing and decreasing PDL along the link

Up to this point the OSNR distribution shape has been analyzed for the cases in which PDL is fixed for all the WSSs and when it is completely aleatory. Based on the outcome of experimental analysis of chapter 4, it can be stated that the reciprocal position in which noise and PDL are inserted is pivotal in determining the kind of penalty that will be suffered due to PDL. Looking at Figure from Figure 4.13 to Figure 4.24, it is clear that the case in which the distributions are more stretched are when the noise is injected at RX side. A larger distribution means an higher PDL penalty, due to the fact that more cases will be far from the mean value, which is the expected one. Such bad cases are all the ones on the negative part of the x-axis. Through the usage of the developed Monte Carlo simulator and thanks to the laboratory observation, it is possible to determine which cases are included in the negative part of the distributions. The experiments indicates that worse results are obtained when PDL is inserter before the noise in the link. This lead to conjecture that the case in which PDL is decreasing among

the WSSs along the link should be worse than when it is increasing, because a larger amount of PDL is injected in the first part of the link. This is reasonable thinking to PDL as a quantity that tends to interfere to itself: when a lot of PDL is injected first, then it is more unlikely that the remaining small contributions will be able to interfere in a destructive way. The opposite when considering a value of PDL which is small at first and then becomes higher and higher.

The current simulation has been performed with the values of PDL depicted in Table 5.1. Such values have been chosen so that their average is equal to 0.2 dB: in this way the average PDL along the link is the same of section 5.1. Decreasing PDL values are obtained by flipping the sequence of increasing values. The total number of runs is also in this case 25000 both for increasing and decreasing PDL.

WSS position	Increasing PDL [dB]	Decreasing PDL [dB]
1	0.03077	0.36923
2	0.06154	0.33846
3	0.09231	0.30769
3	0.09231	0.30769
4	0.12308	0.27692
5	0.15385	0.24615
6	0.18462	0.21538
7	0.21538	0.18462
8	0.24615	0.15385
3	0.27692	0.12308
3	0.30769	0.09231
3	0.33846	0.06154
3	0.36923	0.03077

Table 5.1: Values of increasing and decreasing PDL with respect to their insertion position

The OSNR distributions of this final simulation are provided in Figure form 5.6 to 5.9. As already stated, a distribution is evaluated as "worse" in term of PDL penalty when it is more spread around its mean value, since it is more likely that OSNR will assume values lower than its mean value, which is the expected one. Following this paradigm, it can be asserted that, as expected, the worst case among the two options is when PDL is decreasing among the WSSs. In all the cases, from just a single span to 12, the bell width is higher in the case of decreasing PDL rather than increasing PDL. For instance, focusing on the case of 12 span, the distribution width for decreasing PDL is equal to 0.75 dB, while it is equal to just 0.3 dB for increasing PDL. This outcome is important when trying to derive a

closed formula to obtain the value of PDL penalty to be inserted in the software of GNPy. This additional step is the natural prosecution of this thesis work, and it will be the definitive target in order to include PDL effect in the optical network DT.

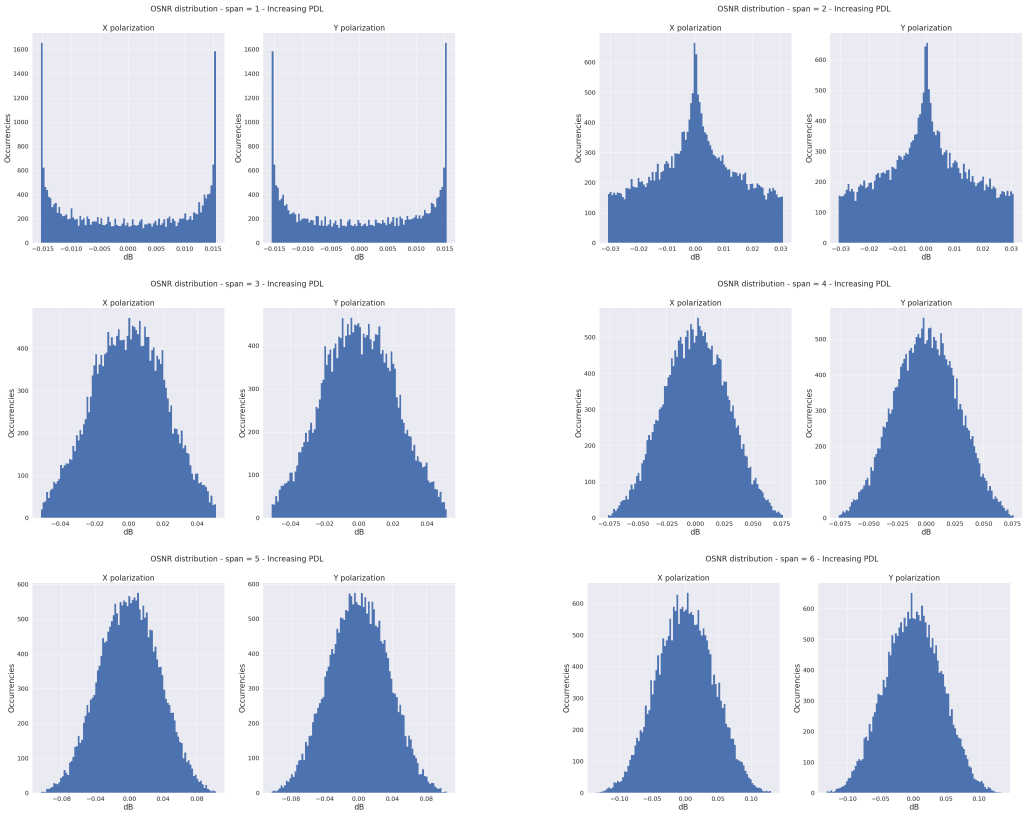

Figure 5.6: Monte Carlo run results for increasing PDL from 1 span to 6

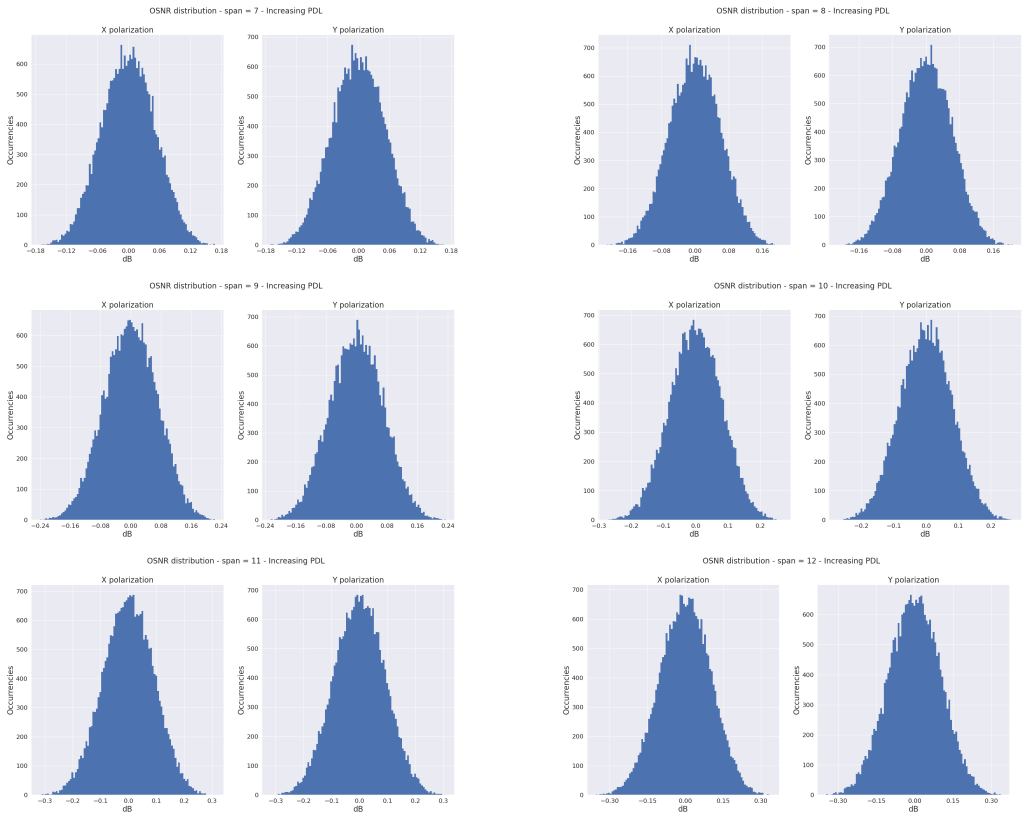

Figure 5.7: Monte Carlo run results for increasing PDL from 7 span to 12

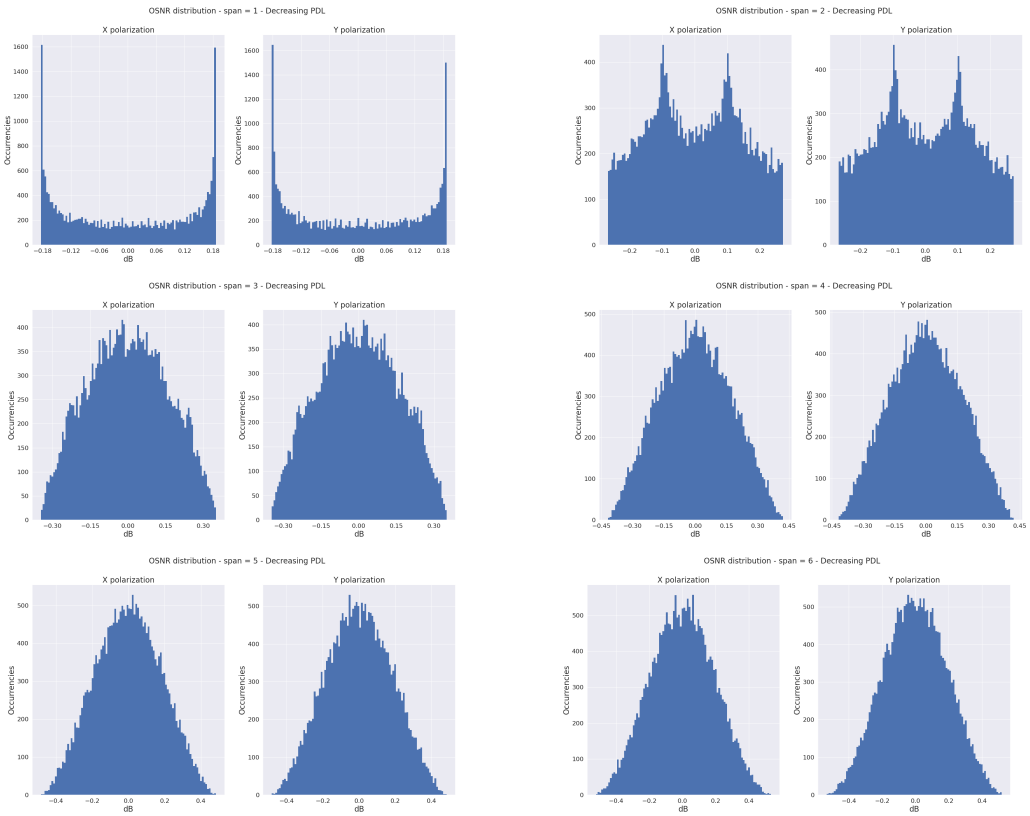

Figure 5.8: Monte Carlo run results for decreasing PDL from 1 span to 6

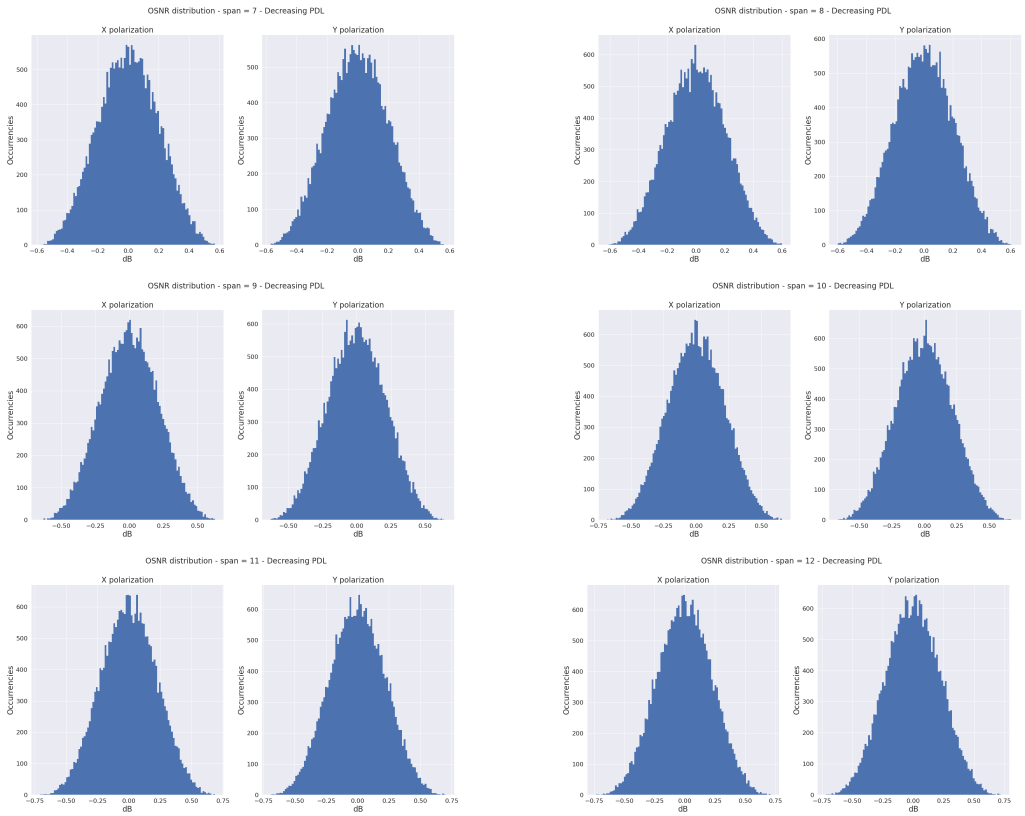

Figure 5.9: Monte Carlo run results for decreasing PDL from 7 span to 12

Chapter 6

Conclusions

The thesis work encompasses the derivation, the experimental analysis and the software implementation of a mathematical model for GSNR computation in presence of PDL, in the framework of open and disaggregated optical networking.

The main conclusions achieved through this discussion are related to many aspects of PDL phenomena that have been observed, in particular:

- The way in which the noise power is affected by PDL can now be easily estimated through a mathematical model based on power transfer matrices, whose correctness has been proved starting from Jones matrices and vectors theory.

- Such mathematical model can be expressed in disaggregated way, and it is suitable to be included in a optical network DT according to the paradigm of open networking, to enable optical NaaS.

- The received GSNR distribution, in presence of PDL effect, takes on a bell shape, which is similar to a gaussian distribution when the number of elements that introduce PDL is large. This effect is emphasized when considering random distributed PDL for each WSS.

- The reciprocal insertion of PDL and noise along a lightpat plays a crucial role in order to determine the impact of PDL on the received GSNR. In particular, the penalty appears to be higher when PDL is inserted before noise, or when it decreases along the path.

- A Monte Carlo simulator, based on the developed mathematical model is now available, and through it it is possible to carry on extensive analysis that would be impossible to held in a laboratory for resources and time reasons.

The experimental measurements have been obtained in the photonics laboratory of LINKS Foundation, and the work has been developed in collaboration with Consortium GARR, thanks to which the results are a further step in open networking tools development, which is the target of BALLOON project.

The outcome of this work is pivotal in the development of an expression of PDL GSNR penalty in closed form, which is the natural prosecution of this thesis. Namely, it will be possible to express the bell distributions width according to a metric based on the statistical characterization of PDL along the path. In this way it will be possible to estimate with a certain degree of probability how much the GSNR will be expected to degradate. Such improvement is important to reach a more efficient exploitation of optical networks, rather than wasting resources considering just the worst case as it is currently done.

Further work can also focus on the experimental validation of such penalty formula for a final implementation on GNPy DT transmission model. This would allow to mark an additional step in treating the transmission model of optical network DT with statistical tools, rather than deterministic ones, which is the more common and simple way, adding completeness and correctness to the DT physical layer abstraction. The final goal that can be achieved with the improvement of GNPy DT is the possibility to implement optical NaaS, switching from an outdated paradigm to a modern, efficient and advanced one.

Bibliography

[1] *Cisco Annual Internet Report*. URL: https://www.cisco.com/c/en/us/solutions/collateral/executive-perspectives/annual-internet-report/white-paper-c11-741490.html (cit. on p. 1).

[2] Yi Zhang, Pulak Chowdhury, Massimo Tornatore, and Biswanath Mukherjee. «Energy Efficiency in Telecom Optical Networks». In: *IEEE Communications Surveys & Tutorials* 12.4 (2010), pp. 441–458. DOI: 10.1109/SURV.2011.062410.00034 (cit. on p. 1).

[3] Gangxiang Shen and Rodney S Tucker. «Translucent optical networks: the way forward [topics in optical communications]». In: *IEEE Communications Magazine* 45.2 (2007), pp. 48–54 (cit. on p. 1).

[4] Marian Marciniak. «Transparency of optical networks: how to manage it?» In: Feb. 1999, pp. 85–88. ISBN: 0-7803-5637-3. DOI: 10.1109/ICTON.1999.781852 (cit. on p. 1).

[5] Riccardo Schips, Roberto Morro, Renato Ambrosone, Stefano Straullu, Francesco Aquilino, Antonino Nespola, Anna Chiadò Piat, and Vittorio Curri. «Enhancing Whitebox Optical SDN Control Using OpenROADM Models». In: *2024 IEEE 25th International Conference on High Performance Switching and Routing (HPSR)*. 2024, pp. 7–12. DOI: 10.1109/HPSR62440.2024.10636006 (cit. on p. 1).

[6] Yongcheng Li, Li Gao, Gangxiang Shen, and Limei Peng. «Impact of ROADM colorless, directionless, and contentionless (CDC) features on optical network performance». In: *Journal of Optical Communications and Networking* 4.11 (2012), B58–B67 (cit. on p. 2).

[7] Wenfeng Xia, Yonggang Wen, Chuan Heng Foh, Dusit Niyato, and Haiyong Xie. «A survey on software-defined networking». In: *IEEE Communications Surveys & Tutorials* 17.1 (2014), pp. 27–51 (cit. on p. 3).

[8] Truong-Xuan Do and Younghan Kim. «Control and data plane separation architecture for supporting multicast listeners over distributed mobility management». In: *ICT Express* 3.2 (2017), pp. 90–95 (cit. on p. 3).

[9] Ramon Casellas, Ricardo Martínez, Ricard Vilalta, and Raül Muñoz. «Metro-haul: SDN control and orchestration of disaggregated optical networks with model-driven development». In: *2018 20th International Conference on Transparent Optical Networks (ICTON)*. IEEE. 2018, pp. 1–4 (cit. on p. 3).

[10] Christian Guillemot et al. «Transparent optical packet switching: The European ACTS KEOPS project approach». In: *Journal of lightwave technology* 16.12 (1998), p. 2117 (cit. on p. 4).

[11] Srinivasan Raghunathan, Ashutosh Prasad, Birendra K Mishra, and Hsihui Chang. «Open source versus closed source: software quality in monopoly and competitive markets». In: *IEEE Transactions on Systems, Man, and Cybernetics-Part A: Systems and Humans* 35.6 (2005), pp. 903–918 (cit. on p. 4).

[12] Fei Hu, Qi Hao, and Ke Bao. «A survey on software-defined network and openflow: From concept to implementation». In: *IEEE Communications Surveys & Tutorials* 16.4 (2014), pp. 2181–2206 (cit. on p. 4).

[13] Emilio Riccardi, Paul Gunning, Óscar González de Dios, Marco Quagliotti, Víctor López, and Andrew Lord. «An operator view on the introduction of white boxes into optical networks». In: *Journal of Lightwave Technology* 36.15 (2018), pp. 3062–3072 (cit. on p. 4).

[14] Vittorio Curri. «GNPy model of the physical layer for open and disaggregated optical networking». In: *Journal of Optical Communications and Networking* 14.6 (2022), pp. C92–C104 (cit. on pp. 5, 7).

[15] Edward Glaessgen and David Stargel. «The Digital Twin Paradigm for Future NASA and U.S. Air Force Vehicles». In: *53rd AIAA/ASME/ASCE/AHS/ASC Structures, Structural Dynamics and Materials Conference*. DOI: 10.2514/6.2012-1818. eprint: https://arc.aiaa.org/doi/pdf/10.2514/6.2012-1818. URL: https://arc.aiaa.org/doi/abs/10.2514/6.2012-1818 (cit. on p. 6).

[16] Vittorio Curri. «Digital-Twin of Physical-Layer as Enabler for Open and Disaggregated Optical Networks». In: *2023 International Conference on Optical Network Design and Modeling (ONDM)*. 2023, pp. 1–6 (cit. on p. 6).

[17] Vittorio Curri. «Is the Digital Twin of the Optical Transport the Enabler for Multi-Band Open and Disaggregated Optical Networks?» In: *2023 23rd International Conference on Transparent Optical Networks (ICTON)*. 2023, pp. 1–4. DOI: 10.1109/ICTON59386.2023.10207279 (cit. on p. 7).

[18] Mark Filer, Mattia Cantono, Alessio Ferrari, Gert Grammel, Gabriele Galimberti, and Vittorio Curri. «Multi-Vendor Experimental Validation of an Open Source QoT Estimator for Optical Networks». In: *J. Lightw. Technol.* 36.15 (Aug. 2018), pp. 3073–3082. DOI: 10.1109/JLT.2018.2818406 (cit. on p. 7).

[19] *https://telecominfraproject.com* (cit. on p. 8).

[20] *GitHub repository of GNPy*. Version v2.0. DOI: 10.5281/zenodo.3458319. DOI: 10.5281/zenodo.3458319. URL: https://doi.org/10.5281/zenodo.3458319 (cit. on p. 8).

[21] Vittorio Curri. «Synergistic Use of AI and Physics Models in Planning and Controlling Multi-Band Optical Networks». In: *2023 IEEE Photonics Conference (IPC)*. 2023, pp. 1–2. DOI: 10.1109/IPC57732.2023.10360570 (cit. on p. 9).

[22] Reza Nejabati, Eduard Escalona, Shuping Peng, and Dimitra Simeonidou. «Optical network virtualization». In: *15th International Conference on Optical Network Design and Modeling-ONDM 2011*. IEEE. 2011, pp. 1–5 (cit. on p. 9).

[23] Jonathan Homa and Krishna Bala. «ROADM architectures and their enabling WSS technology». In: *IEEE Communications Magazine* 46.7 (2008), pp. 150–154 (cit. on p. 11).

[24] Yiran Ma, Luke Stewart, Julian Armstrong, Ian G. Clarke, and Glenn Baxter. «Recent Progress of Wavelength Selective Switch». In: *Journal of Lightwave Technology* 39.4 (2021), pp. 896–903. DOI: 10.1109/JLT.2020.3022375 (cit. on pp. 11, 13).

[25] Ivan Kaminow, Tingye Li, and Adam Willner. *Optical Fiber Telecommunications, Components and Subsystems*. Academic Press, 2013. ISBN: 978-0-12-396958-3. DOI: https://doi.org/10.1016/C2011-0-06843-6 (cit. on p. 12).

[26] Andrea D'Amico, Giacomo Borraccini, Stefano Straullu, Francesco Aquilino, Stefano Piciaccia, Alberto Tanzi, Gabriele Galimberti, and Vittorio Curri. «Statistical Analysis of PDL Penalty on Coherent Transmission Technologies Based on WSS Experimental Characterization». In: *2022 Asia Communications and Photonics Conference (ACP)*. 2022, pp. 874–877. DOI: 10.1109/ACP55869.2022.10088670 (cit. on pp. 15, 40, 65, 66, 69).

[27] Andrea D'Amico, Giacomo Borraccini, Stefano Straullu, Francesco Aquilino, Stefano Piciaccia, Alberto Tanzi, Gabriele Galimberti, and Vittorio Curri. «Experimental probing and modeling of the PDL impact on the optical signal-to-noise ratio». In: *Optical Fiber Communication Conference*. Optica Publishing Group. 2023, W1E–6 (cit. on p. 15).

[28] Andrea D'Amico et al. «Analytical Models and Artificial Intelligence for Open and Partially Disaggregated Optical Networks». In: *Politecnico di Torino* (2023), pp. 1–189 (cit. on pp. 15, 17).

[29] N Gisin. «Statistics of polarization dependent losses». In: *Optics Communications* 114.5 (1995), pp. 399–405. ISSN: 0030-4018. DOI: https://doi.org/10.1016/0030-4018(95)00687-4. URL: https://www.sciencedirect.com/science/article/pii/0030401895006874 (cit. on p. 16).

[30] A. El Amari, N. Gisin, B. Perny, H. Zbinden, and C.W. Zimmer. «Statistical prediction and experimental verification of concatenations of fiber optic components with polarization dependent loss». In: *Journal of Lightwave Technology* 16.3 (1998), pp. 332–339. DOI: 10.1109/50.661358 (cit. on p. 16).

[31] B. Huttner, C. Geiser, and N. Gisin. «Polarization-induced distortions in optical fiber networks with polarization-mode dispersion and polarization-dependent losses». In: *IEEE Journal of Selected Topics in Quantum Electronics* 6.2 (2000), pp. 317–329. DOI: 10.1109/2944.847767 (cit. on p. 16).

[32] Y. Fukada. «Probability density function of polarization dependent loss (PDL) in optical transmission system composed of passive devices and connecting fibers». In: *Journal of Lightwave Technology* 20.6 (2002), pp. 953–964. DOI: 10.1109/JLT.2002.1018806 (cit. on p. 16).

[33] A. Galtarossa and L. Palmieri. «The exact statistics of polarization-dependent loss in fiber-optic links». In: *IEEE Photonics Technology Letters* 15.1 (2003), pp. 57–59. DOI: 10.1109/LPT.2002.805799 (cit. on p. 16).

[34] A. Mecozzi and M. Shtaif. «Signal-to-noise-ratio degradation caused by polarization-dependent loss and the effect of dynamic gain equalization». In: *Journal of Lightwave Technology* 22.8 (2004), pp. 1856–1871. DOI: 10.1109/JLT.2004.832424 (cit. on p. 16).

[35] Lynn Nelson, Cristian Antonelli, Antonio Mecozzi, Martin Birk, Peter Magill, Anton Schex, and Lutz Rapp. «Statistics of polarization dependent loss in an installed long-haul WDM system». In: *Optics express* 19 (Mar. 2011), pp. 6790–6. DOI: 10.1364/OE.19.006790 (cit. on p. 16).

[36] Segev Zarkosvky and Mark Shtaif. «Statistical distribution of polarization-dependent loss in systems characterized by the hinge model». In: *Optics Letters* 45 (Feb. 2020). DOI: 10.1364/OL.385525 (cit. on pp. 16, 17, 25).

[37] Dennis Goldstein. *Polarized light: Third edition*. Dec. 2017, pp. 1–770. ISBN: 9781315217789. DOI: 10.1201/b10436 (cit. on p. 20).

[38] Richard Gilbert. «The General-Purpose Interface Bus.» In: *IEEE Micro* 2.1 (1982), pp. 41–51 (cit. on p. 35).

[39] *Cisco WXC datasheet*. URL: https://www.cisco.com/c/en/us/products/collateral/optical-networking/network-convergence-system-2000-series/data_sheet_c78-729313.pdf (cit. on p. 36).

[40] *Novoptel polarimeter datasheet*. URL: https://www.novoptel.de/Polarimeter/PM1000_flyer.pdf (cit. on p. 37).

[41] *Novoptel polarization scrambler datasheet*. URL: https://www.novoptel.de/Scrambling/EPS1000_flyer.pdf (cit. on p. 37).

[42] *Keysight Tunable Laser datasheet*. URL: https://www.keysight.com/us/en/assets/7018-01142/data-sheets-archived/5988-8518.pdf (cit. on p. 38).

[43] *Thorlabs polarization scrambler datasheet*. URL: https://www.thorlabs.de/thorproduct.cfm?partnumber=PL100S (cit. on p. 39).

[44] *Agilent polarization scrambler datasheet*. URL: https://www.artisantg.com/TestMeasurement/47786-1/Keysight-Agilent-11896A-Polarization-Controller?srsltid=AfmBOoqs8GmEfw1a_xlHcAVn8d86ceeR1lTKQvAM46KY2zlKtrhJ4Lpq (cit. on p. 39).

[45] Andrea D'Amico et al. «GNPy Experimental Validation in a C+L Multiband Optical Multiplex Section». In: *2024 24th International Conference on Transparent Optical Networks (ICTON)*. 2024, pp. 1–4. DOI: 10.1109/ICTON62926.2024.10648172 (cit. on p. 54).

[46] Vittorio Curri. «Software-defined WDM optical transport in disaggregated open optical networks». In: *2020 22nd International Conference on Transparent Optical Networks (ICTON)*. IEEE. 2020, pp. 1–4 (cit. on p. 54).